tech ops

EXPERIMENTAL STUDY OF SCATTERING IN REAL ATMOSPHERES

By Ralph G. Eldridge and John C. Johnson

REPORT NO. TO-B 59-16

CONTRACT NO. AF 19(604)-2175

December 30, 1959

Prepared for

GEOPHYSICS RESEARCH DIRECTORATE
AIR FORCE CAMBRIDGE RESEARCH CENTER
AIR RESEARCH AND DEVELOPMENT COMMAND
UNITED STATES AIR FORCE
BEDFORD, MASSACHUSETTS

TECHNICAL OPERATIONS INCORPORATED

EXPERIMENTAL STUDY OF SCATTERING IN REAL ATMOSPHERES

By

Ralph G. Eldridge
and
John C. Johnson

REPORT NO. TO-B 59-16
FINAL REPORT ON
CONTRACT NO. AF 19(604)-2175

DECEMBER 30, 1959

Prepared for

GEOPHYSICS RESEARCH DIRECTORATE
AIR FORCE CAMBRIDGE RESEARCH CENTER
AIR RESEARCH AND DEVELOPMENT COMMAND
UNITED STATES AIR FORCE
BEDFORD, MASSACHUSETTS

D-161

Burlington, Massachusetts

ACKNOWLEDGEMENTS

We wish to acknowledge the efforts and cooperation of many of our co-workers who spent many cold, wet, and cheerless nights on Plum Island to obtain the raw data that forms the basis of this report. In particular we wish to express our appreciation to David K. Beaver, Nancy R York, and Northeastern University students, C. Ellis, J. Sullivan and R. Smith,for their technical assistance in making the field measurements.

CONTENTS

LIST OF FIGURES

ABSTRACT

The scattering of visible light in hazes and fogs was investigated experimentally, using balloon-borne flash bulb clusters as sources and calibrated cameras as detectors. By defocusing the cameras, measurements of both the direct and the scattered components could be obtained on the same film. Several detectors were stationed on the ground at various distances up to 15 kms from the source.

Results indicate that transmission of the direct components decrease exponentially and as the inverse square of the slant range R, while scattered radiation transmission can be described by a different exponential and the inverse first power of the slant range. All transmission constants can be related to the visibility at the time of measurement. Brightness of the aureole surrounding the source decrease inversely as $R^2 \sin^2 \Theta$, where Θ is the angular distance from the source as seen by the observer. This is an average relationship applying at all distances and fog densities observed.

A general expression for the total flux from a point source reaching an observer is given in terms only of the visibility and the slant range.

I. INTRODUCTION

Evaluations of the effect of various meteorological scattering media on radiant energy transport in the atmosphere have been attempted both theoretically and experimentally.

Theoretical studies generally follow the line of reasoning which specifies model atmospheres with homogeneous strata. These approaches are not without merit, because they indicate the manner in which light is transmitted through various scattering media. The weakness in these approaches seems to be that the models may be relatively unrealistic: i.e., real atmospheres are not homogeneous, and radiant energy transfer may be influenced by losses upward and out of the atmosphere and by reflections from surfaces whose albedoes are not well known.

Experimental approaches to this problem can be instructive by indicating the flux density received from a point source through distances of several kilometers for those weather situations encountered. The diffuse transmission through real atmospheres as measured by photometers with fields of view of about 150° was reported earlier by the authors (References 1 and 2). This study indicated the general trends that the transmission assumes. However, the relationship between the direct and scattered components of the total transmission is unknown because the photometers measured total flux only.

The subject of this final report is a study which was aimed at determining the behavior of the direct and scattered components of the total transmission through various scattering media, as well as the possible contribution of reflections from the intervening terrain. The results are discussed in terms of the actual measurements, with an indication of how they may be applied to direct beam measurements made in similar atmospheres by other workers. Finally an attempt has been made to relate the experimental results to theoretical parameters and a simple model atmosphere.

II. INSTRUMENTATION

The principle adopted here for the measurement of both direct and scattered components of the flux arriving from a concentrated source was one in which both could be simultaneously determined. The detection equipment consisted simply of cameras and film, with auxiliary apparatus needed to make the system acceptably quantitative. Because the light sources consisted of 50 cm diameter clusters of photoflash bulbs, operated at distances of at least several hundred meters, their images would have been extremely small on the film in a conventional camera. Moreover, their brightnesses would have far exceeded the maximum which the film could record. To obviate these difficulties, the cameras were deliberately defocused to the point where the source produced a measurably large circle of confusion on the film. The effect of defocusing on the resolution of the system was such that scattering of 2^{o} or less could not be distinguished from the direct beam. Since the wide angle scattering was of major interest, this loss of resolution was judged acceptable.

Six pairs of cameras were located at various distances from a balloon-borne light source. The balloon flight was tracked with the camera shutters open until after the flash occurred. As a result, the exposure was given by the lens aperture times the flash pulse duration, superimposed on the illuminance of the background. The experiments were performed at night to reduce the background illumination to a minimum. The photographic technique also allowed evaluation of the background brightness and other terrestrial lights.

The source consisted of 30 No. 50 photoflash bulbs symmetrically arranged and connected to fire simultaneously. Based on information furnished by the manufacturer, and a measured configuration efficiency of 0.85, the energy emitted by the source was 2.4×10^{6} lumen-seconds in the visible spectrum, or 12 kilocalories over the entire 3800^{o}K black-body spectrum. This emerged in a triangular pulse of 40 milliseconds duration, with a peak emittance of 1.3×10^{8} lumens, or 2.4 megawatts.

Films exposed during the field experiments were previously masked along the edge. The resulting unexposed section of film was later exposed to a calibrated step wedge illuminated by an electronic flash source whose duration had been made equal to the field photoflash source. These films were then developed at constant temperature with nitrogen burst

agitation. All negatives exposed to the same source were developed together to obtain as much uniformity as possible. Analysis of each sheet of film consisted of reading the optical densities of the step wedge and constructing an H and D curve. The measured optical densities of the flash image were referred to this H and D curve to determine the corresponding exposures.

The cameras used were B and J 4 x 5 Press View Cameras with Schneider-Kreuznach Xenar f/3.5, 105 mm lens in Synchro-Compur-P shutter, operated about 1 cm off focus. The film pack adapters were modified to mask off one end of the film for later exposure to the calibrated step wedge. All exposures in the field were made at f/3.5, with the exposure time determined by the pulse duration of the photoflash bulbs.

The detector-source combination used, Kodak Tri-X film in the pack form and No. 50 photoflash bulbs, exhibit relatively flat spectral response between 0.42 and 0.64 micron, with a slight maximum occurring at about 0.61 micron wavelength. The film response cuts off at 0.36 and 0.67 micron wavelength (Reference 3).

Beside the necessity for film calibration, use of cameras and film for photometry also requires determining (1) the relationship between the optical density and the source intensity; (2) the efficiency of the lens as a function of incident angle, and (3) the relative sensitivity of each camera. Each of these factors will influence the accuracy of measurement of the atmospheric transmissions. The techniques and experiments performed to evaluate and control these problems are discussed below.

A. FILM CALIBRATION

Calibration of Kodak Tri-X film was accomplished by exposing an edge of the film to a gray step wedge illuminated by a modified electronic flash unit. The electronic flash tube was mounted at one end of a light-tight blackened tube and a film holder was attached at the other end. The physical features of the flash sensitometer are shown in Figure 1. A sheet of film is placed in the film slot so that the masked end is laid against the calibrated step wedge. The felt-lined cover is pressed down, holding the film in place, and the flash tube is triggered. The film is then removed and placed on a hanger for eventual development along with other films in that particular experimental transmission measurement The film is processed in total darkness, from removal from the film pack holder to complete "fixing" after development.

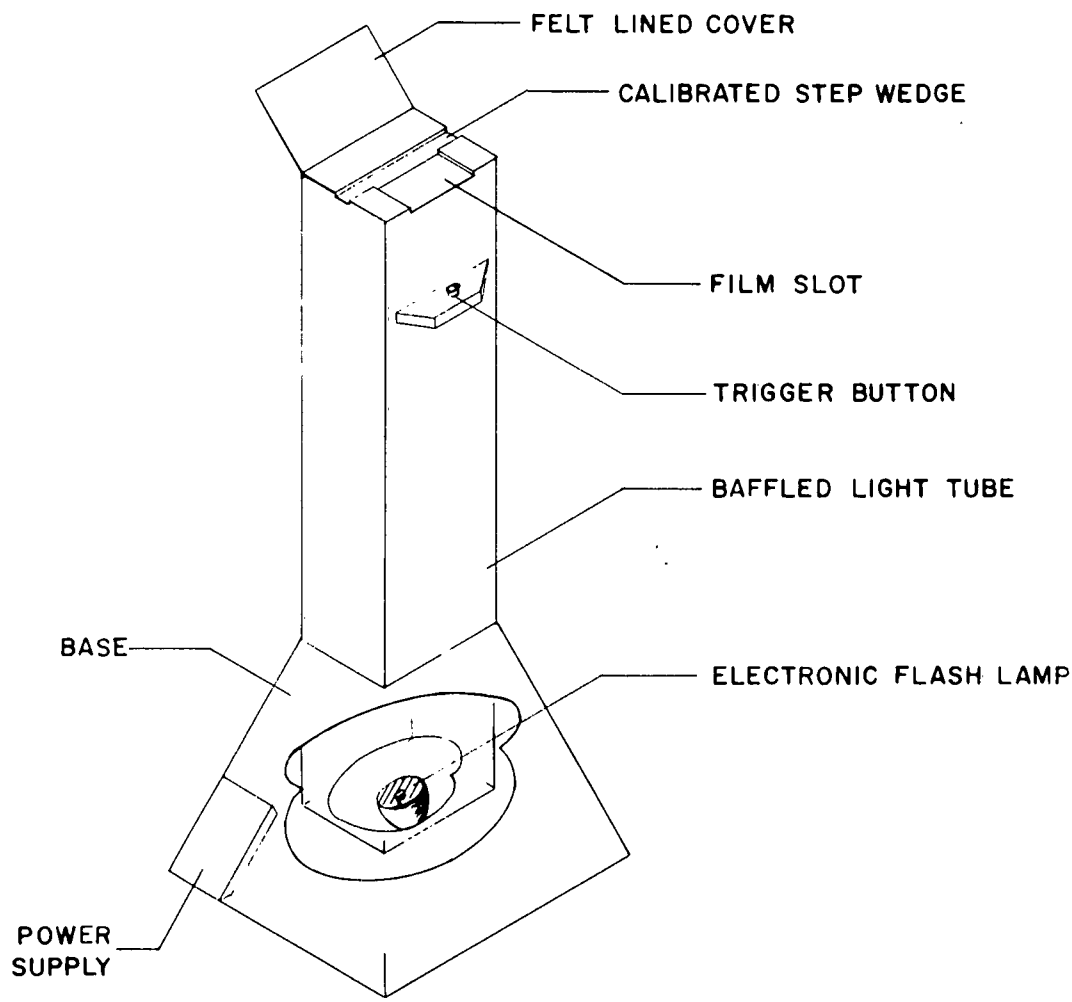

FIGURE 1
FLASH SENSITOMETER

Because of the marked difference between the pulse length of a standard electronic flash and that of a photoflash bulb, the electronic flash was modified to approximate the time duration of the photoflash bulbs. By adding resistance in series with the flash lamp, the discharge was slowed down to about 30 milliseconds. Independent measurements of the pulse length in the visible range had previously indicated this to be the approximate pulse length of the photoflash bulbs.

The flash sensitometer was tested for reproducibility by measuring the light output with an integrating photometer. The variation about a mean value was 2% for 30 measurements of the total visible integrated flux. This error is well within the limits to which the film optical densities can be measured with the densitometer being used.

The gray step wedge used in the sensitometer was a standard semi-transparent film wedge purchased from the Welch Scientific Company. This wedge is normally used to calibrate the Welch Densichron instrument. The range of densities was increased by covering one edge of the wedge with a neutral density filter made from uniformly exposed film. The features of the modified step wedge are shown in Figure 2. The neutral density filter is mounted along the left side of the wedge; the numbers on the right edge are the step wedge numbers. The optical densities, ρ, are listed, as well as relative log exposure, beside each step.

All negatives from which data were derived were developed with nitrogen burst agitation at a constant temperature. An indication of the constancy of development was obtained by monitoring the resultant H and D curves for each sheet of film as a function of chronological time. The films were developed 19 minutes at 68°F in Kodak DK 50 developer, giving a gamma of about 0.9. A typical H and D curve is shown in Figure 3. The relative log exposure of each step (Figure 2) is indicated on the abscissa of Figure 3. The overlap of steps is a consequence of the choice of the neutral filter.

A comparison of 12 H and D curves indicates an average variation of 0.026 optical density unit with a maximum variation of 0.035 optical density unit where the overlap occurs. This results in a maximum uncertainty of 0.08 in relative log exposure units. Part of this uncertainty results from inaccuracy in measuring the optical density, and produces a variation in the relative log exposure of 0.05 unit. This value is considered more representative, because the overlap magnifies the uncertainty. The atmospheric trans-

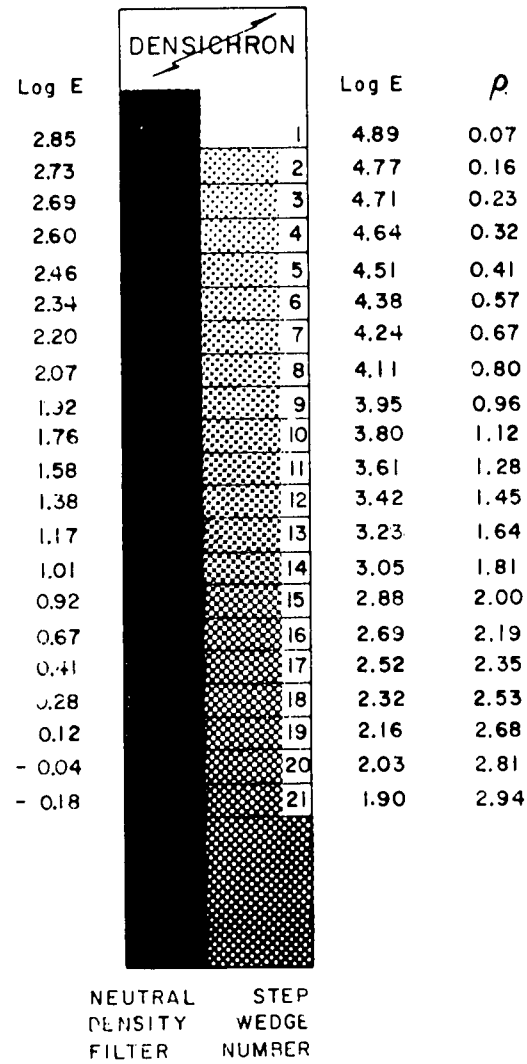

FIGURE 2
CALIBRATING STEP WEDGE

FIGURE 3

TYPICAL H & D CURVE CALIBRATION

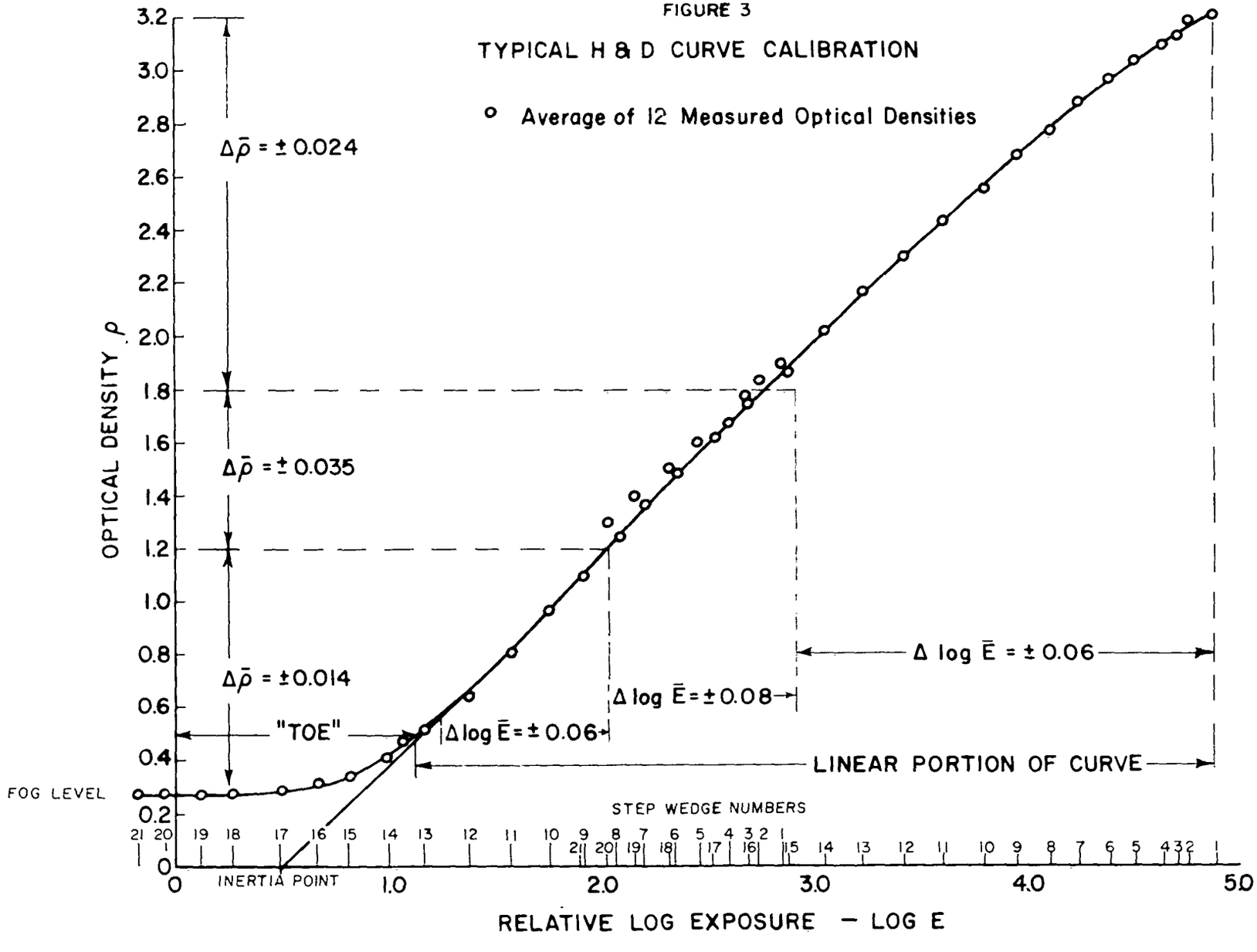

mission data were obtained through most of the linear portion of the curve; however, because each relative log exposure is derived through the H and D curve for each sheet of film, data can be obtained throughout the H and D curve provided the optical density is above the fog level and below the level of overexposure. In practice, care was exercised to determine that neither of these limits was exceeded. These uncertainties also contribute to the experimental error, and are reflected in the atmosphere transmissions.

An examination was made of the effect of differences in color temperatures of the electronic flash lamp source used in the sensitometer and of the photoflash bulb sources used in the field experiments. This possibility of error was investigated by exposing film to both sources through the step wedge. Results normalized in the linear portion of the H and D curve are shown diagramatically in Figure 4. Except at the lower end of the exposure scale, the comparison of light sources indicates that the use of an electronic flash lamp source in the sensitometer introduces only a negligible error in the calibrations of the film. This conclusion is, of course, valid only with Kodak Tri-X (panchromatic) film and the particular electronic flash tube and No. 50 photoflash bulbs (color temperatures about 6000°K and 3800°K, respectively).

B. CAMERA CALIBRATION

Calibration of the cameras required the measurement of two major parameters: (1) lens transmission as a function of incident angle for each camera; (2) relative sensitivity of each camera.

The camera lens was calibrated by making photographs of a fluorescent lamp, chosen because of its relatively uniform brightness. The films were developed with nitrogen burst agitation after exposure to the calibration wedge. The brightness of the fluorescent lamp was measured along the longitudinal axis at the points where densitometric measurements of the lamp's image were to be made. The results are summarized in graphic form for all cameras in Figure 5. The ordinate is the lens efficiency, equal to the normalized ratio of image to lamp brightness; the abscissa is the lateral distance from the center of the film. It may be seen that the experimental data depart from the theoretical rate of decrease proportional to $\cos^4 \Phi$, where $\tan \Phi$ distance from center/image distance from lens. However, it is not uncommon for experimental lens efficiencies to deviate from this value

FIGURE 4

COMPARISON OF H & D CURVES
RESULTANT FROM EXPOSURE OF KODAK
TRI-X FILM TO DIFFERENT SOURCES

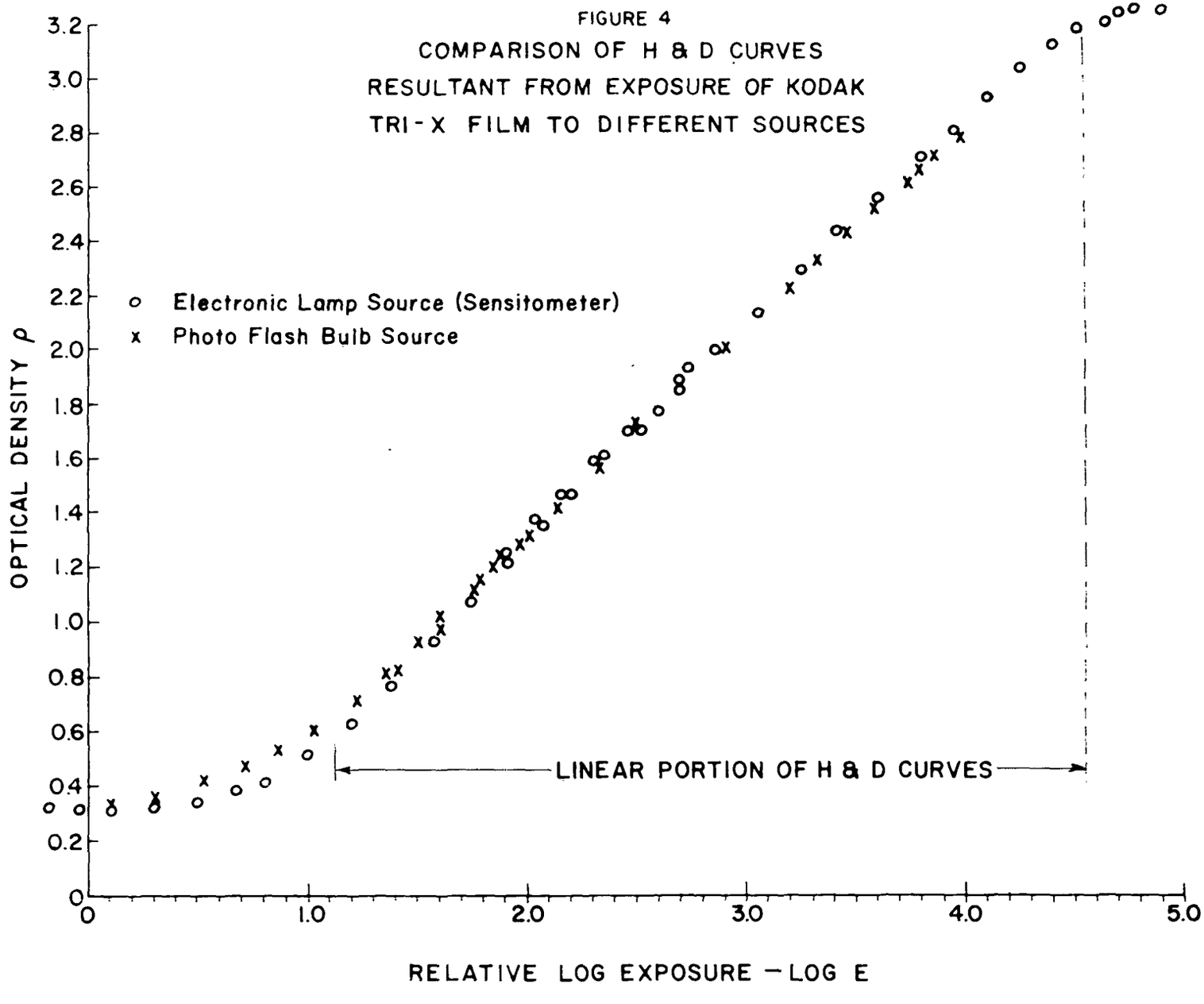

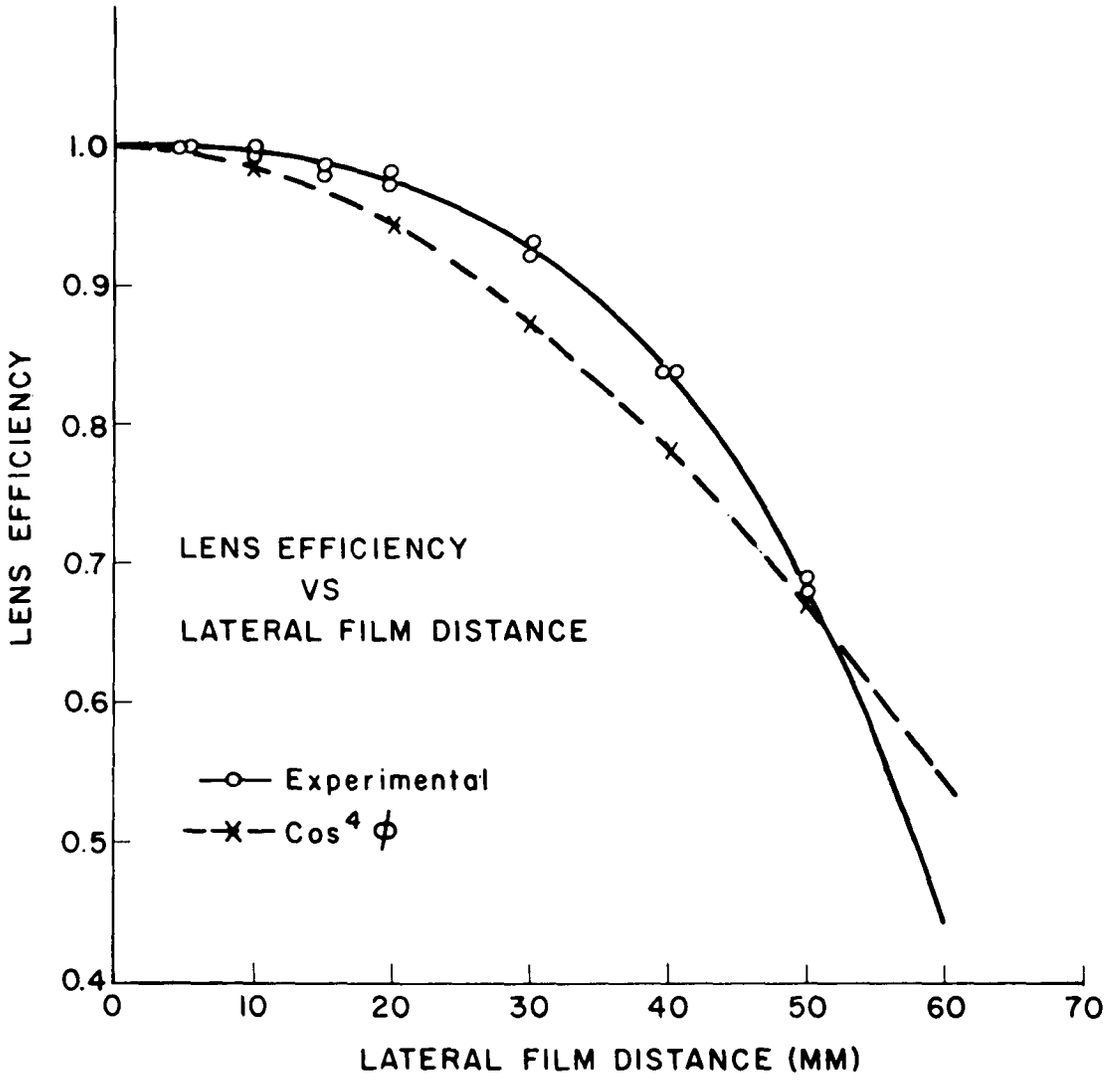
LENS EFFICIENCY
1.0
0.9
0.8
0.7
0.6
0.5
0.4
LENS EFFICIENCY
VS
LATERAL FILM DISTANCE
Experimental
Cos⁴ φ
0
10
20
30
40
50
60
70
LATERAL FILM DISTANCE (MM)

FIGURE 5

(Reference 4). The experimental curve indicates that some vignetting is present. The experimental lens efficiency curve is used to correct the source image density according to the image distance from the center of the film.

The relative sensitivity of each camera was determined by observing the same flash source simultaneously with all the cameras at the same range under field conditions. All cameras were set up at one location to observe seven flashes in succession. The resulting negatives were developed as described and the relative flux density for each flash was obtained by the procedure detailed below. The relative sensitivity, S, for any one camera is defined as the quotient of the average flux density measured by all the cameras and the flux density measured by the given camera. For each camera, standard deviation of the individual sensitivities derived from each flash is shown in Table I in the column headed by σ_i . This is a measure of the system errors, excluding variations in the source intensity, and it can be seen that they are gratifyingly small.

TABLE I

CAMERA RELATIVE SENSITIVITIES

Camera	S	σ_i , %
1	0.96	1.23
2	1.05	0.80
3	1.04	0.60
4	1.02	0.57
5	1.01	0.57
6	0.95	0.93
7	0.99	1.06
8	0.96	0.90
9	0.97	0.52
10	1.02	0.97
11	1.01	0.97
12	1.02	1.30
Average	1.00	0.87

C. EXPERIMENTAL PROCEDURE

All field experiments were performed at night on Plum Island, Newburyport, Massachusetts. (For a detailed description of balloon and source techniques used here, see Reference 1.) Cameras were mounted in pairs on a swivel support so that they could be aimed in azimuth and elevation. The 12 cameras were distributed at five or six different distances from the launching site of the balloon-borne photoflash bulb source. When the balloon was released, a pilot light was tracked with each set of cameras. The shutters were opened after launching prior to the flash, and closed immediately after the flash. The balloon was also tracked with two theodolites situated 1.26 km apart. Each theodolite determined the azimuth and elevation angle of the flash with respect to the mutual base line, and from these data the heights of the flashes were calculated (see Table II). Similarly, the horizontal position of each flash was calculated to within ± 0.02 km, and from this the slant ranges from the flash to each camera were determined by triangulation.

TABLE II

MEASURED HEIGHTS OF SOURCES

Flash	Height (km)	Deviation	Atmosphere
A	0.268	± 0.013	Light haze
B	0.225	± 0.015	Light haze
C	0.468	± 0.023	Light haze
D	0.190	± 0.030	Moderate haze
E	0.220	± 0.015	Dense haze and smoke
F	0.19	± 0.05	Dense fog
G	0.14	± 0.08	Dense fog
H	0.13	± 0.08	Dense fog

The heights given for the flash in dense fog are less accurate, due to the extreme difficulty in tracking. The pilot light was visible for only a short time before it disappeared into the fog, and indicated only roughly where the flash occured in space. In those cases the theodolite was used to determine the point where the pilot light disappeared

from view, after which the course of the balloon was extrapolated to the time of firing.

The largest variable in the experiment was the brightness of the photoflash bulb source. The percentage variance of the source brightness was determined from the same data previously used to determine the individual camera sensitivities. Using these seven flashes, the variance of the flux density is 25%. However, because the flux from each flash was measured at several ranges, the absolute value of the source was not needed to determine relative transmission between stations.

When each field experiment was completed, the films from each camera were extracted from the film packs and grouped according to the flash. The calibration wedge was exposed on each film, and then all 12 sheets of film were developed together. As a result, the only uncontrolled variables remaining in the experiment were the photoflash source intensity and the atmosphere. Source variations could be eliminated by extrapolating the unscattered component to zero distance; thus the measured quantities should be functions only of the atmosphere.

III. DATA REDUCTION

After a series of negatives had been developed, the optical density of the central image, ρ_D, and the optical density at specific distances from the central image, ρ_S, were measured with a Welch Densichron Densitometer. The general features of negatives for the three major atmosphers encountered are shown in Figure 6. The high optical density at the center of the nearly concentric rings represents the defocused source image; the rings about this image represent lines of equal optical density. In general, the scattered or diffuse energy is circularly symmetric about the source in atmospheres of haze, and somewhat elliptically symmetrical in an atmosphere of fog. In practice, the optical density is measured in the four quadrants from the source image along the horizontal and vertical axis at 0.25, 0.50, 0.75, 1.0, 1.5, 2.0, 3.0, 4.0, etc., mm from the image when the atmosphere is hazy. However, because the diffuse energy is not symmetrical in foggy atmospheres, the optical density of a negative representing a source in fog is measured on a 10-mm grid centered on the source image. These optical densities are converted into log exposure by means of the H and D curve for that particular piece of film. The unscattered component of the light incident on the camera is the product of the exposure, E_D, and the area of the central image, A_D. The scattered energy is the product of the exposure, E_S, and the area of the grid of density measurements observed.

The direct and scattered fluxes, respectively, are determined as follows:

$$D_{obs} = E_D A_D S_C F; \tag{3.1}$$

and

$$S_{obs} = E_S A_S S_C F; \tag{3.2}$$

where:

E_D and E_S are the exposures for the direct and scattered energies for the pulse duration of the photoflash bulbs;

A is the area over which the optical densities ρ_D and ρ_S are measured;

S_c is the relative sensitivity factor for each particular camera; and

F is the filter factor when a neutral density filter is used over the lens.

FIGURE 6

TYPICAL OPTICAL DENSITIES OF NEGATIVE
REPRESENTING THE THREE ATMOSPHERES

LIGHT HAZE
SLANT RANGE - 3.28 Km

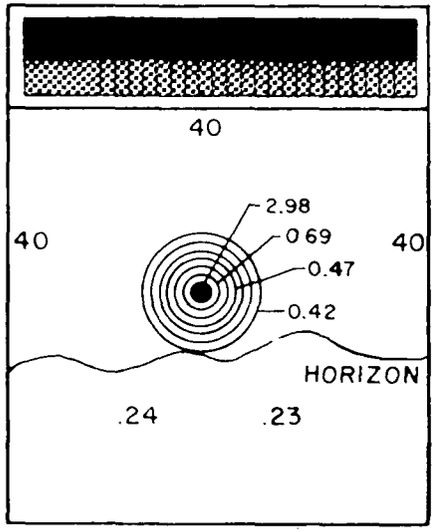

DENSE HAZE AND SMOKE
SLANT RANGE - 1.49 Km

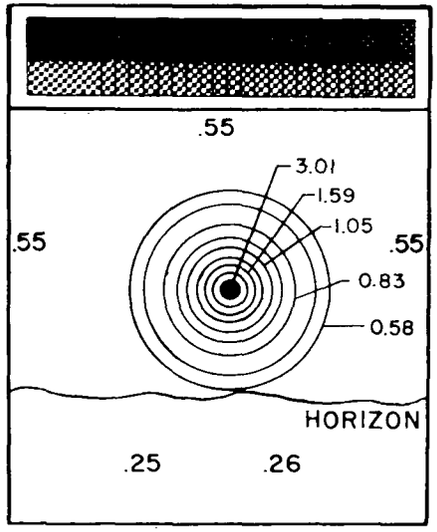

DENSE FOG
SLANT RANGE - 0.24

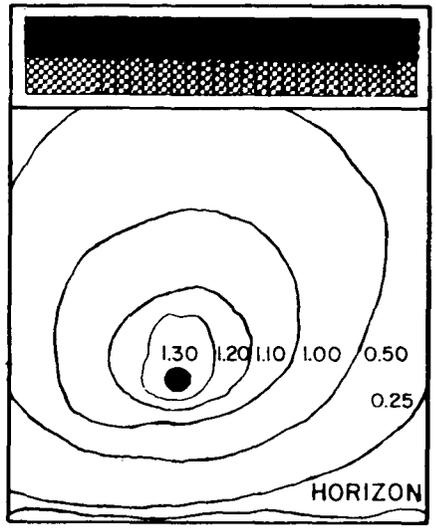

The neutral density filters were used to prevent overexposure when the source was measured at ranges less than 1.5 km. These filters were procured from Eastman Kodak Company who specified the optical densities to be within 1% of the values 1.0, 2.0, 3.0 and 4.0 for each filter.

During the field experimental phase of this study 10 flashes were fired for atmospheric transmission measurements. Two of these were discarded: one was observed by an insufficient number of cameras to yield significant results; the other was obviously in error in the determination of the flash position in space. Therefore, eight measurements of the total transmission are presented: three for very light haze, one for moderate haze, one for dense haze and smoke, and three for dense fog.

IV. RANGE DEPENDENCE OF DIRECT AND SCATTERED FLUX

Measurements of the direct and scattered flux reaching the cameras are presented in Figures 7 through 14 as functions of the slant range, R. The solid curves represent the data multiplied by R^2 to correct for inverse square dependence and were thus converted to quantities proportional to transmission. The direct flux in all cases can be seen to be attenuated exponentially in its passage through the atmosphere. The scattered flux, however, is not depleted so simply. Theoretical analysis (Reference 5) of the behavior of radiation singly scattered by a homogeneous medium indicates that this intensity should decrease exponentially and approximately inversely with the distance, especially in the neighborhood of the source. Based on this theoretical consideration, the scattered components were multiplied by R and replotted as dashed curves on Figures 7 through 14. It is clear that this quantity is well represented by a straight line on the semi-logarithmic plots.

Accordingly, the total flux arriving at a detector whose slant range is R kilometers from an isotropic source could be described analytically as the sum of two components, the direct flux and the scattered flux:

$$T = D + S, \tag{4.1}$$

where T is the total flux, D and S are the direct and scattered fluxes, respectively. Numerically, D, S, and T are the fluxes from a source which would give unit flux at unit distance in vacuum. The direct flux is then:

$$D = \frac{D_{obs}}{(DR^2)_o} = \frac{e^{-\sigma R}}{R^2} \tag{4.2}$$

where σ is the direct flux extinction coefficient. Results for each test are normalized by dividing all the observed fluxes by the extrapolated value of (DR^2) at zero distance. This appears to be a justifiable procedure, not only theoretically but also as a result of Middleton's experiments (Reference 6); it results from the assumption of strict exponential (and inverse square) attenuation of the unscattered flux from the source. Middleton's work also

shows that σ is identical with the atmospheric extinction coefficient.

The scattered flux may be described as:

$$S = \frac{S_{obs}}{(DR^2)_o} = b \frac{e^{-k_S R}}{R} \tag{4.3}$$

where k_S is the scattered flux extinction coefficient. Combining equations (4.2) and (4.3) equation (4.1) can be written as:

$$T = \frac{e^{-\sigma R}}{R^2} + b \frac{e^{-k_S R}}{R} \tag{4.4}$$

One other quantity of interest must be defined in the same terms. The apparent brightness of the aureole in the photographs is readily derivable from the densitometric data. This quantity, B (R, Θ), is expressed as flux per steradian subtended at the detector, unit flux being defined as before. As an approximation, the brightness was averaged over rings of constant angle Θ away from the line joining source and observer, and is generally a function of Θ and of slant distance, R.

The experimental values of σ, k_S, and b are shown in Table III for each of the eight flashes. These quantities were obtained by a least squares analysis of the experimental data shown in Figures 7 through 14, with the exception of the value of σ for flashes F and G. In these two cases the visibility was so low that only the stations closest to the source were able to measure the direct flux, hence the unambiguous straight line could not be drawn for the quantity DR^2 vs R in Figures 12 and 13. As an approximation, it is assumed that the source intensities for flashes F and G were identical with falsh H, taken within two hours of flash F and one hour of flash G; and from this the value of k_D and b, σ could be inferred.

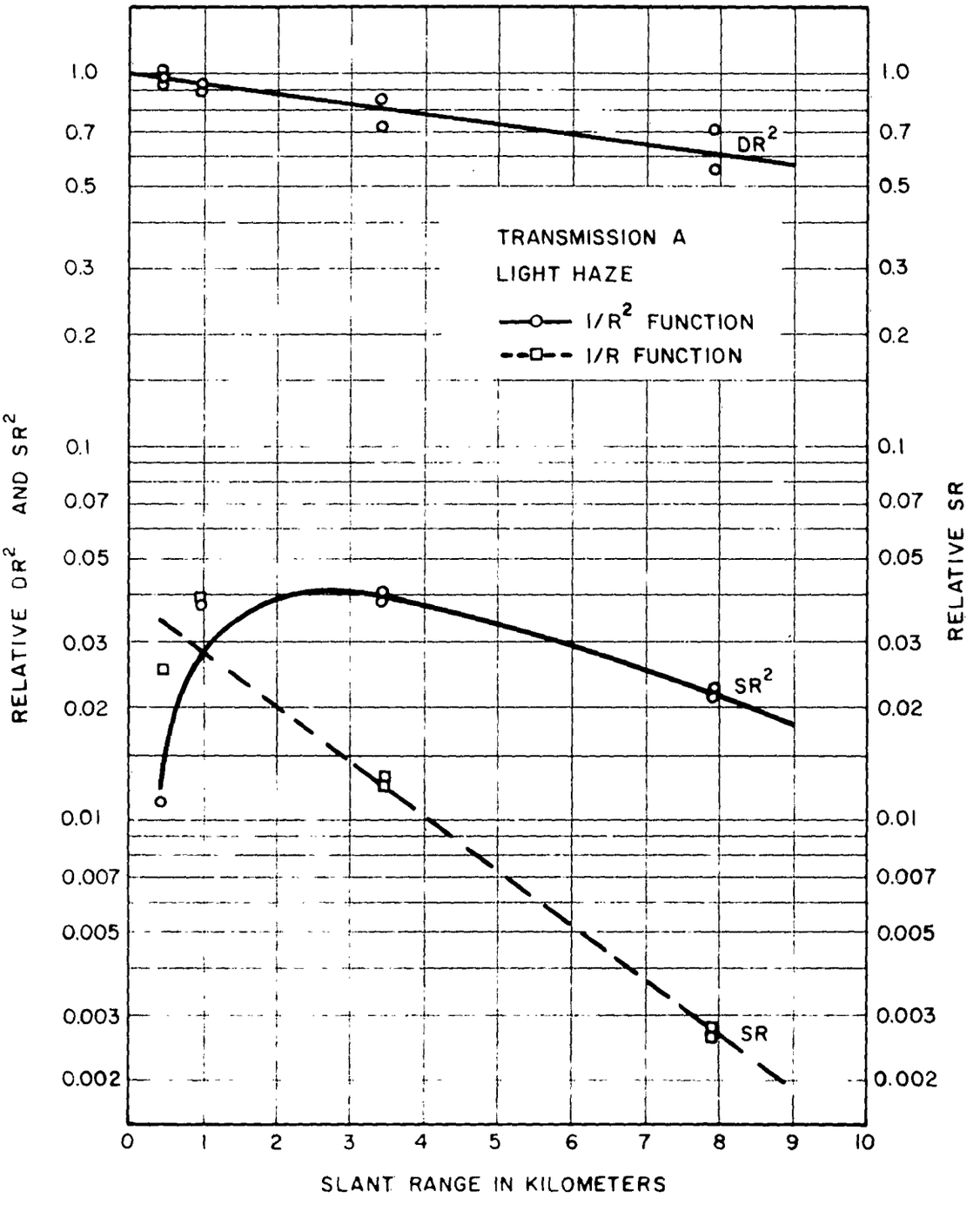
TRANSMISSION A
LIGHT HAZE
1/R² FUNCTION
1/R FUNCTION
DR²
SR²
SR
RELATIVE DR² AND SR²
RELATIVE SR
SLANT RANGE IN KILOMETERS
1.0
0.7
0.5
0.3
0.2
0.1
0.07
0.05
0.03
0.02
0.01
0.007
0.005
0.003
0.002
0
1
2
3
4
5
6
7
8
9
10

FIGURE 7

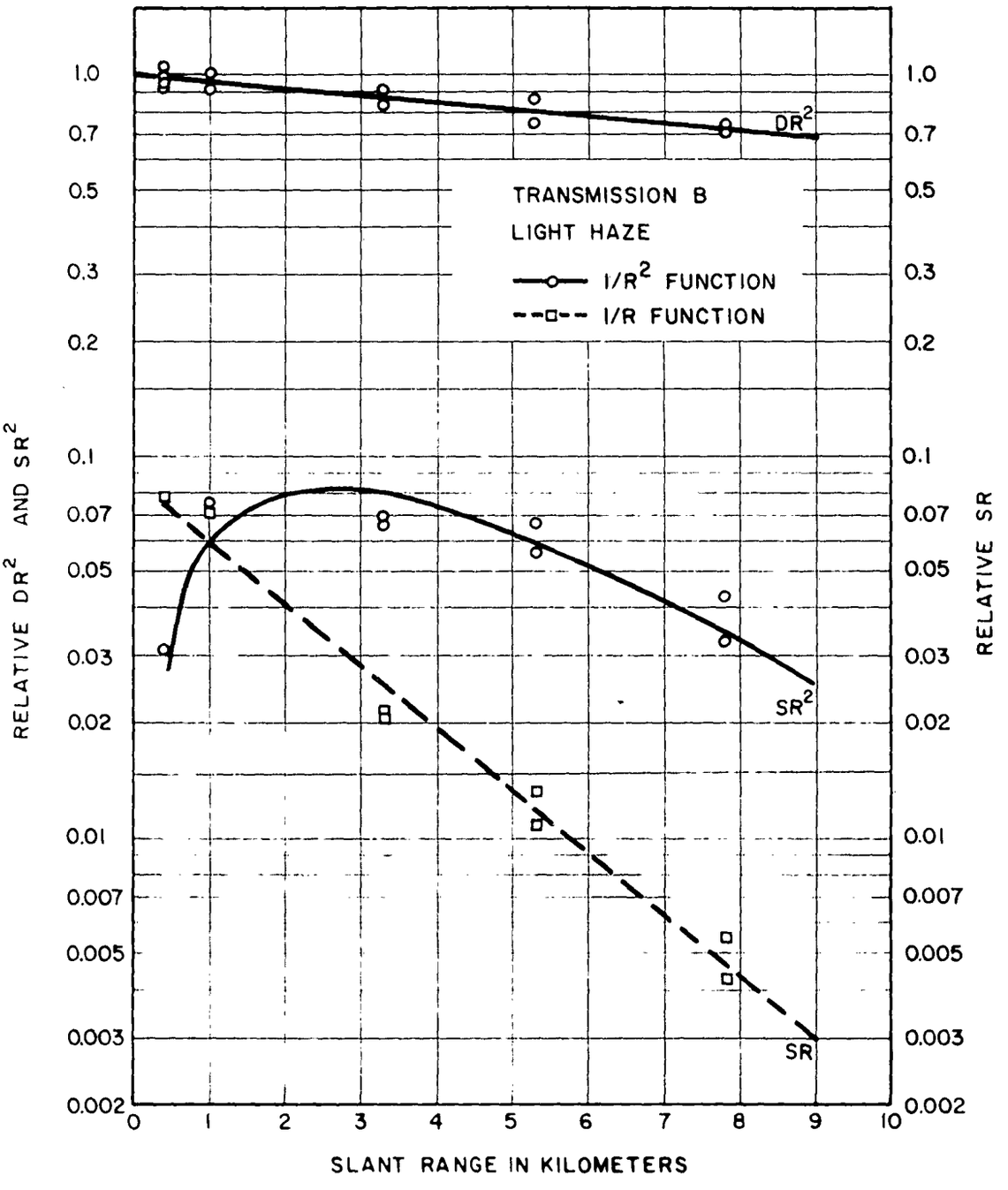
TRANSMISSION B
LIGHT HAZE
1/R² FUNCTION
1/R FUNCTION
DR²
SR²
SR
RELATIVE DR² AND SR²
RELATIVE SR
SLANT RANGE IN KILOMETERS
1.0
0.7
0.5
0.3
0.2
0.1
0.07
0.05
0.03
0.02
0.01
0.007
0.005
0.003
0.002
0
1
2
3
4
5
6
7
8
9
10

FIGURE 8

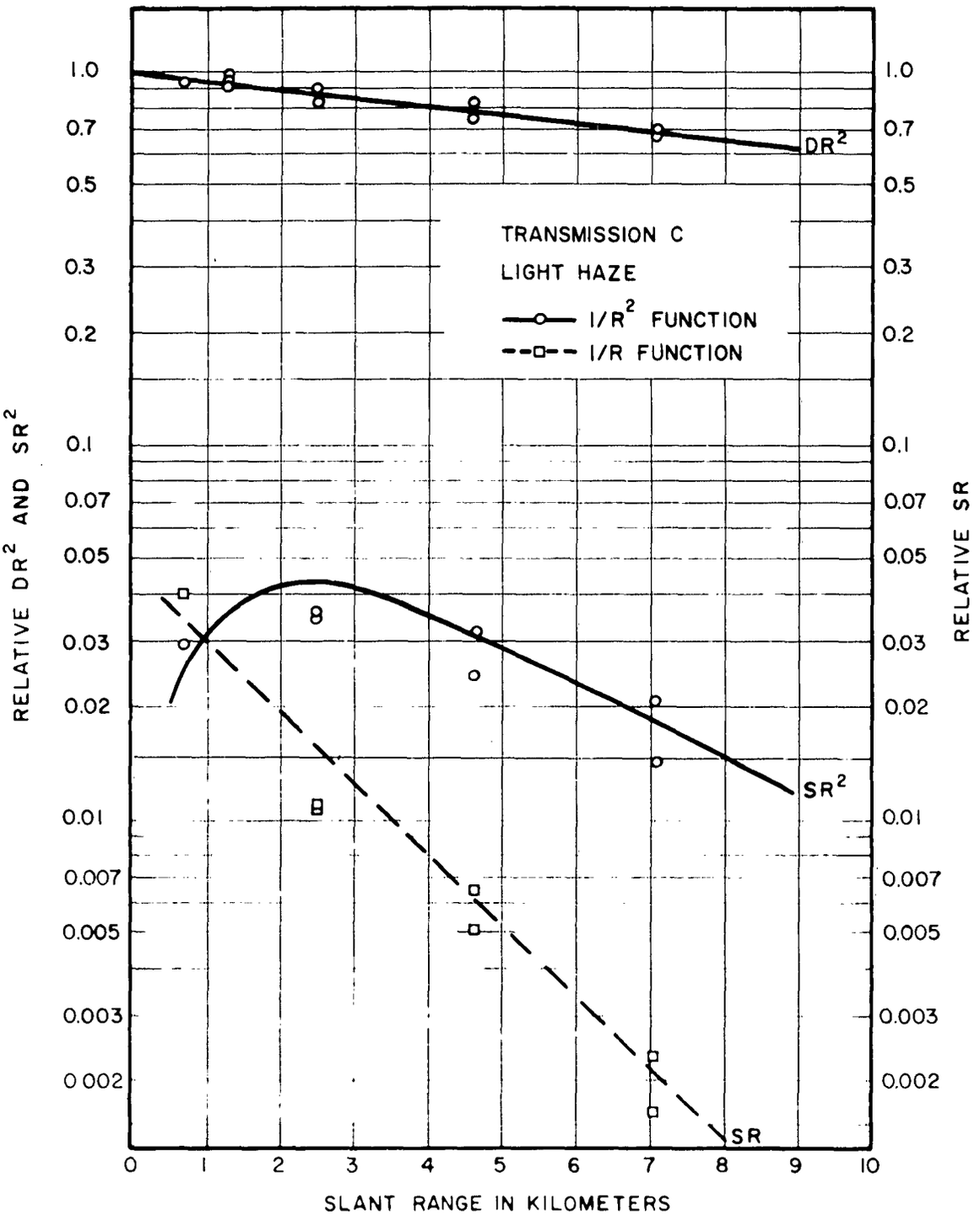
TRANSMISSION C
LIGHT HAZE
1/R² FUNCTION
1/R FUNCTION
DR²
SR²
SR
8
8
RELATIVE DR² AND SR²
RELATIVE SR
SLANT RANGE IN KILOMETERS
1.0
0.7
0.5
0.3
0.2
0.1
0.07
0.05
0.03
0.02
0.01
0.007
0.005
0.003
0 002
0
1
2
3
4
5
6
7
8
9
10

FIGURE 9

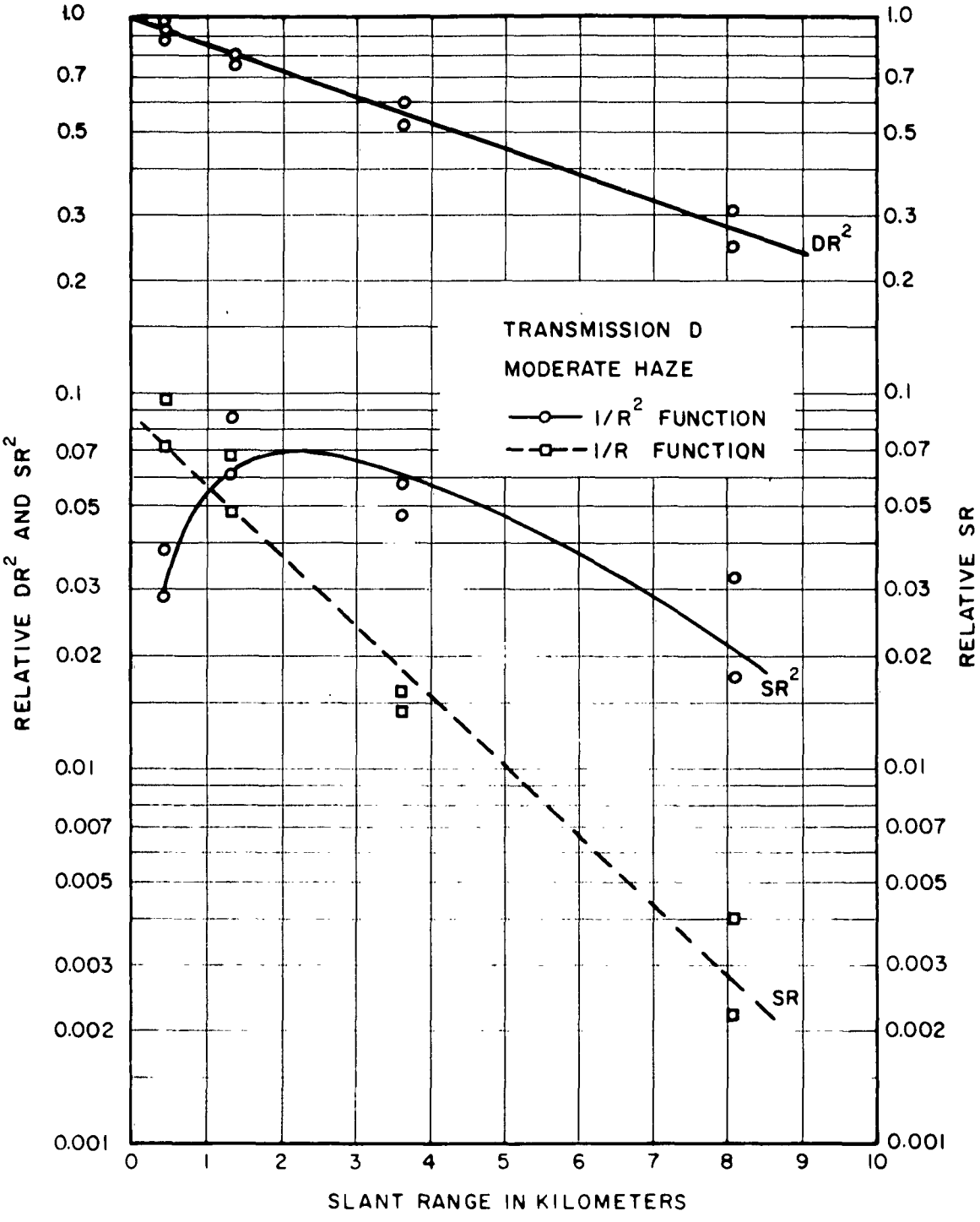
TRANSMISSION D
MODERATE HAZE
1/R² FUNCTION
1/R FUNCTION
DR²
SR²
SR
RELATIVE DR² AND SR²
RELATIVE SR
SLANT RANGE IN KILOMETERS
1.0
0.7
0.5
0.3
0.2
0.1
0.07
0.05
0.03
0.02
0.01
0.007
0.005
0.003
0.002
0.001
0
1
2
3
4
5
6
7
8
9
10

FIGURE 10

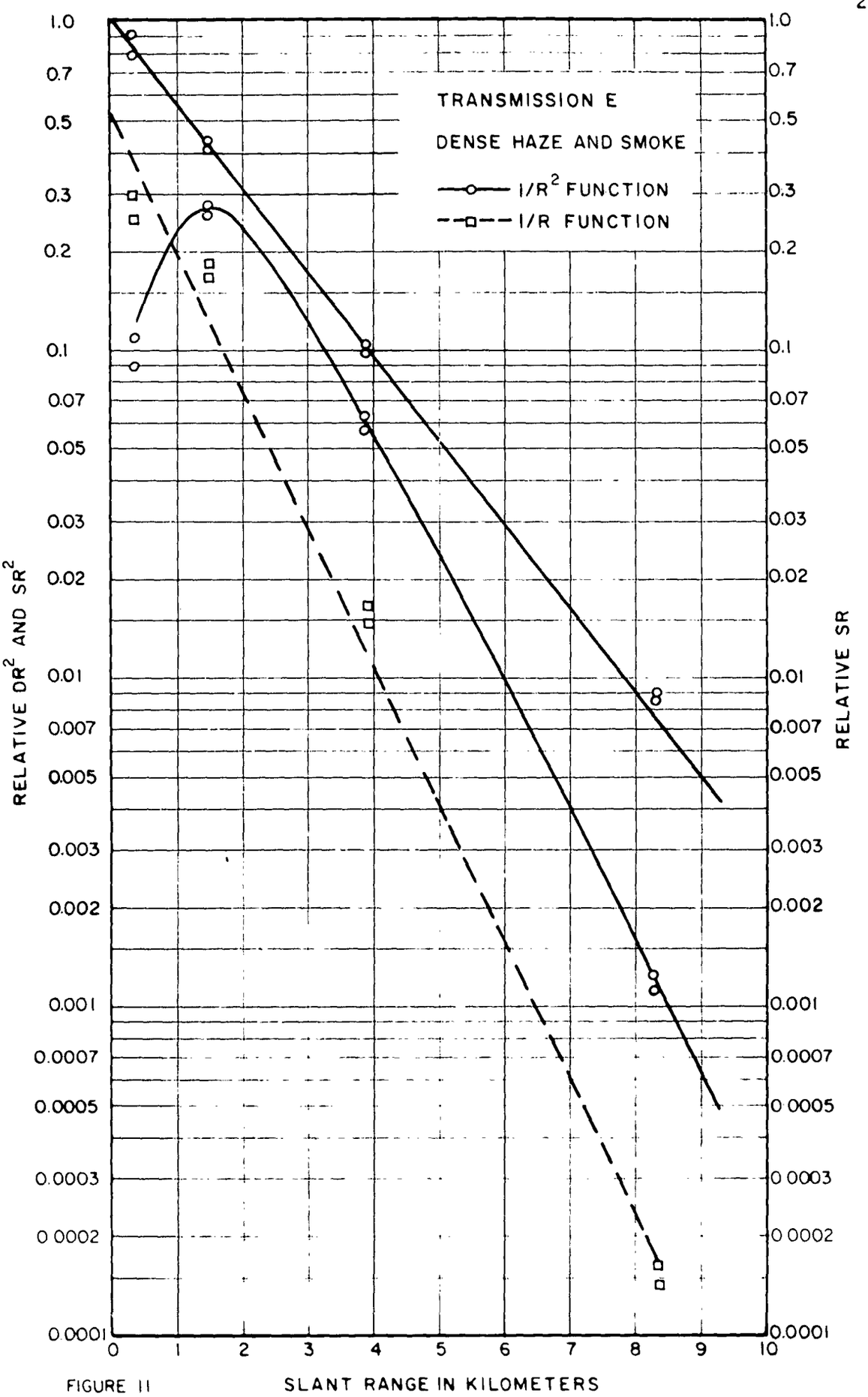
TRANSMISSION E
DENSE HAZE AND SMOKE
I/R² FUNCTION
I/R FUNCTION
RELATIVE DR² AND SR²
RELATIVE SR
SLANT RANGE IN KILOMETERS
1.0
0.7
0.5
0.3
0.2
0.1
0.07
0.05
0.03
0.02
0.01
0.007
0.005
0.003
0.002
0.001
0.0007
0.0005
0.0003
0 0002
0.0001
0
1
2
3
4
5
6
7
8
9
10

FIGURE 11

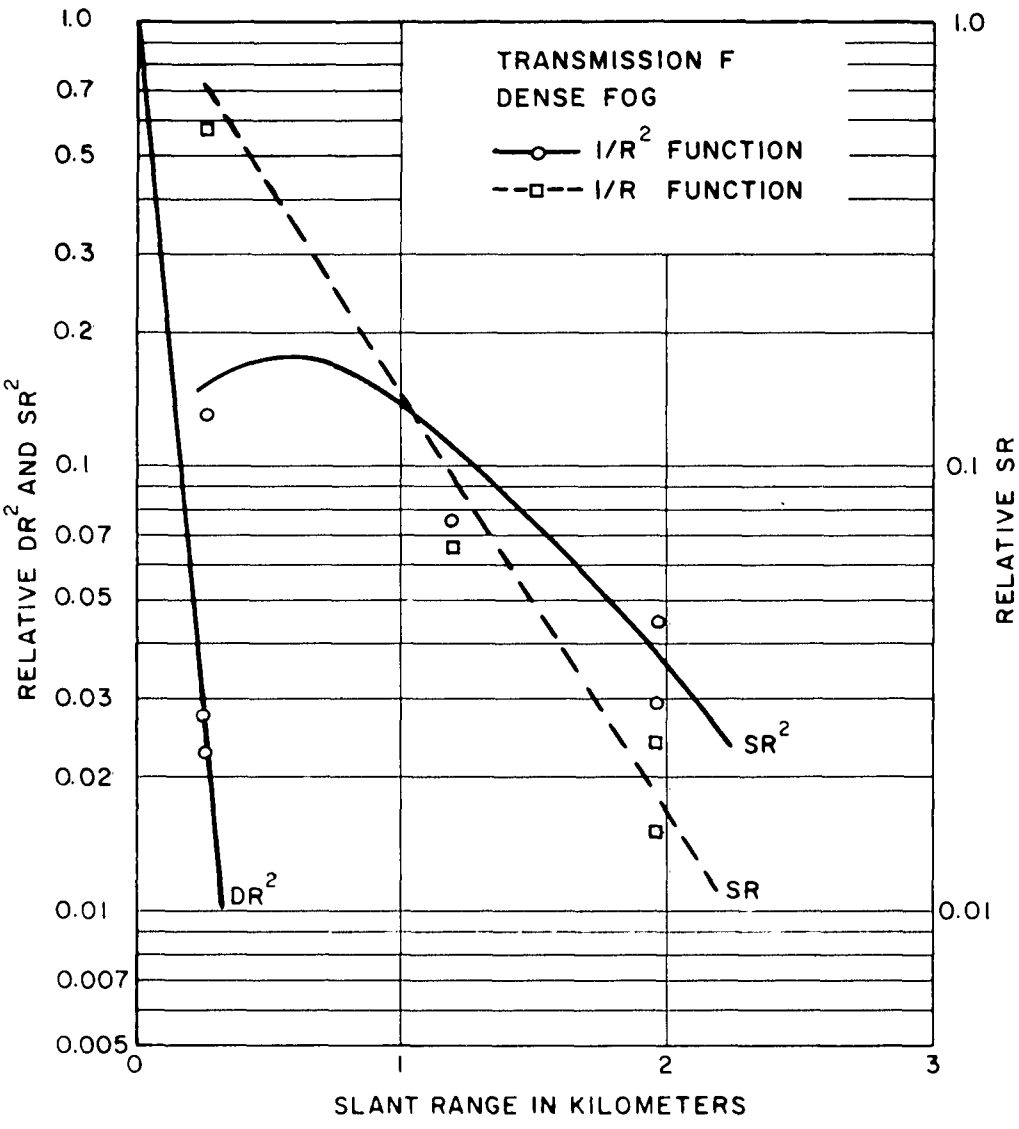
TRANSMISSION F
DENSE FOG
1/R² FUNCTION
1/R FUNCTION
RELATIVE DR² AND SR²
RELATIVE SR
SLANT RANGE IN KILOMETERS
DR²
SR²
SR
1.0
0.7
0.5
0.3
0.2
0.1
0.07
0.05
0.03
0.02
0.01
0.007
0.005
0
1
2
3

FIGURE 12

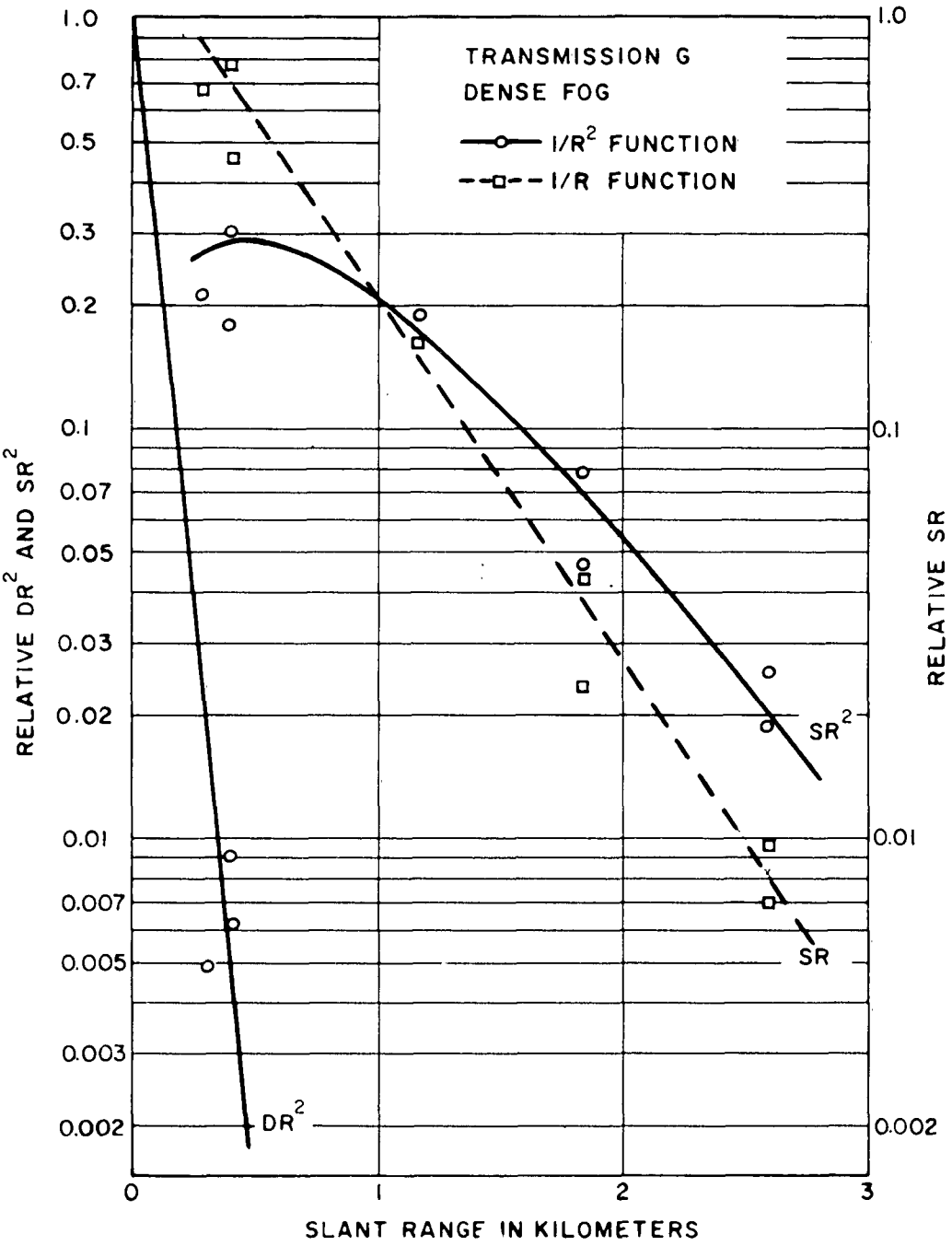
TRANSMISSION G
DENSE FOG
1/R² FUNCTION
1/R FUNCTION
RELATIVE DR² AND SR²
RELATIVE SR
SLANT RANGE IN KILOMETERS
SR²
SR
DR²
1.0
0.7
0.5
0.3
0.2
0.1
0.07
0.05
0.03
0.02
0.01
0.007
0.005
0.003
0.002
0
1
2
3

FIGURE 13

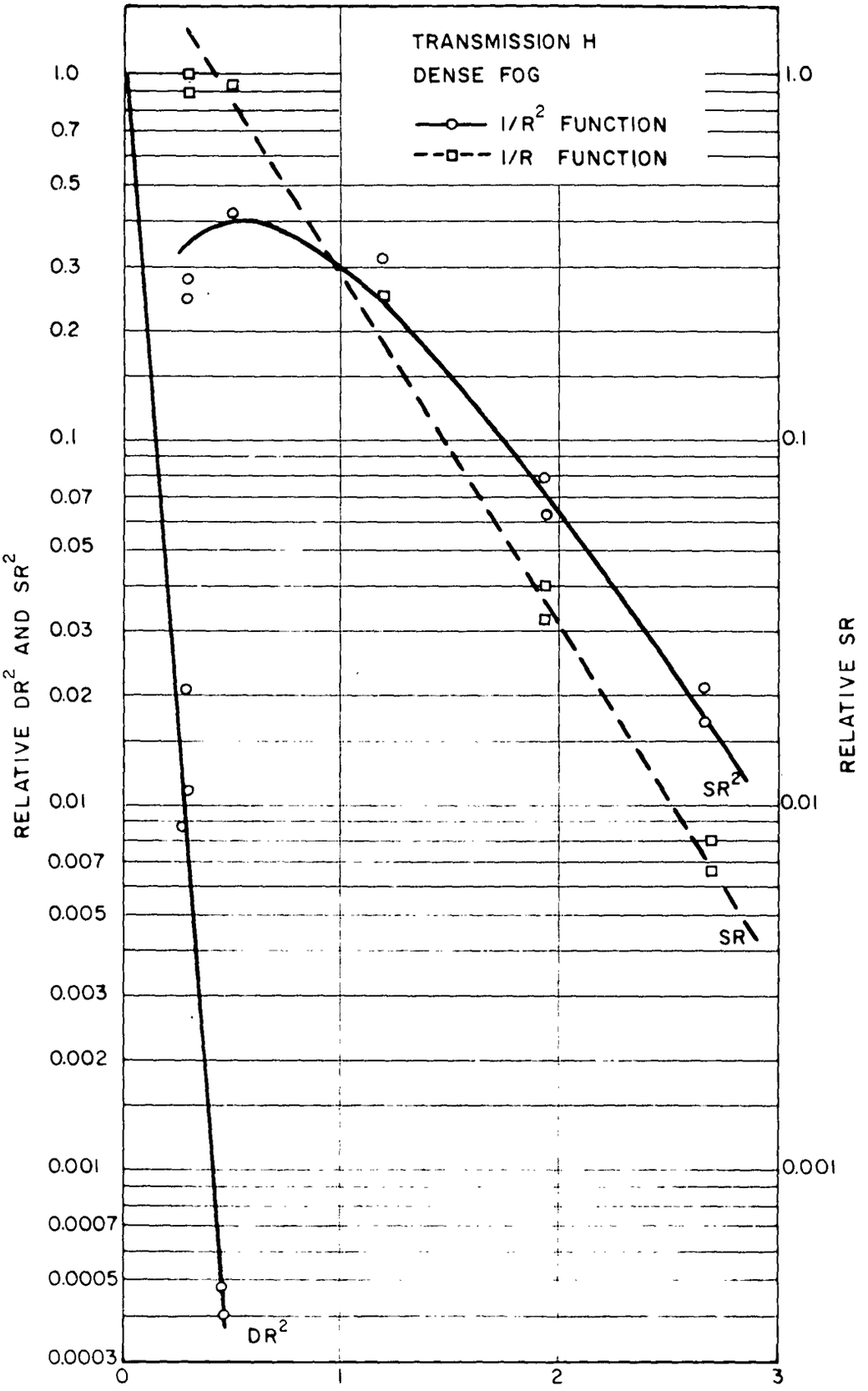
TRANSMISSION H
DENSE FOG
1/R² FUNCTION
1/R FUNCTION
RELATIVE DR² AND SR²
RELATIVE SR
SLANT RANGE IN KILOMETERS
DR²
SR²
SR
1.0
0.7
0.5
0.3
0.2
0.1
0.07
0.05
0.03
0.02
0.01
0.007
0.005
0.003
0.002
0.001
0.0007
0.0005
0.0003
0
1
2
3

FIGURE 14

TABLE III

TRANSMISSION PARAMETERS

Flash	Meteorological Description	σ (km^{-1})	k_S (km^{-1})	b
A	Light haze	0.065	0.34	0.040
B	Light haze	0.043	0.38	0.085
C	Light haze	0.052	0.44	0.047
D	Moderate haze	0.16	0.43	0.009
E	Dense haze and smoke	0.58	0.96	0.52
F	Dense fog	15.1	1.90	1.4
G	Dense fog	13.2	1.91	2.2
H	Dense fog	15.9	2.05	3.9

It was gratifying to find that σ for the three flashes agreed with each other within ± 10%.

It is of interest to determine the dependence of the scattered flux extinction coefficient upon the direct flux extinction coefficient. The simplest form of this dependence, as illustrated in Figure 15, is:

$$k_S = \sigma^{1/3} \tag{4.5}$$

As the parameter b of equation (4.3) is quite sensitive to the experimental data, the dependence of b upon the direct flux extinction coefficient was determined for those atmospheres which obviously had significant scattered energy. For this reason the dependence of b on σ was investigated only for the three cases of fog, dense haze, and smoke, and moderate haze; results are shown in Figure 16. It may be noted that this does not introduce excessive error for the three cases of light haze. The equation of a simple dependence of the parameter b upon the direct flux extinction coefficient is:

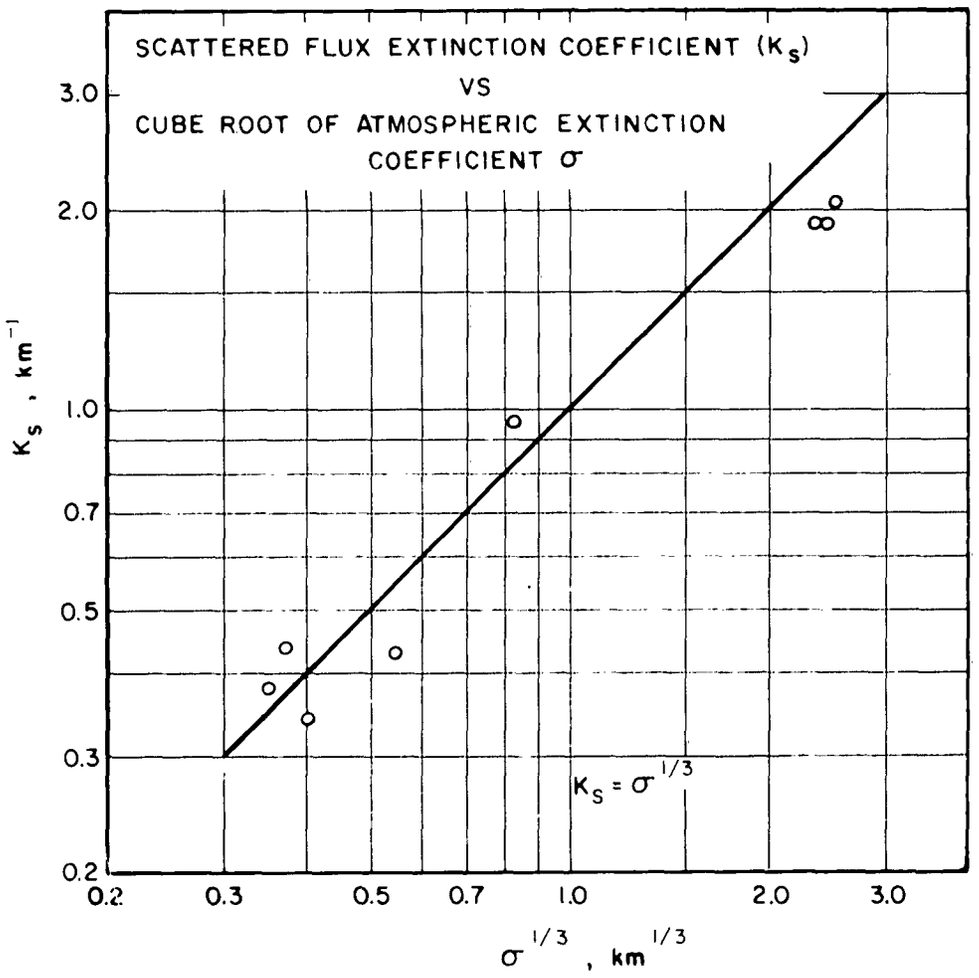
SCATTERED FLUX EXTINCTION COEFFICIENT (K_s)
VS
CUBE ROOT OF ATMOSPHERIC EXTINCTION
COEFFICIENT σ
$K_s = \sigma^{1/3}$
K_s , km^{-1}
$\sigma^{1/3}$, $km^{1/3}$
3.0
2.0
1.0
0.7
0.5
0.3
0.2
0.2
0.3
0.5
0.7
1.0
2.0
3.0

FIGURE 15

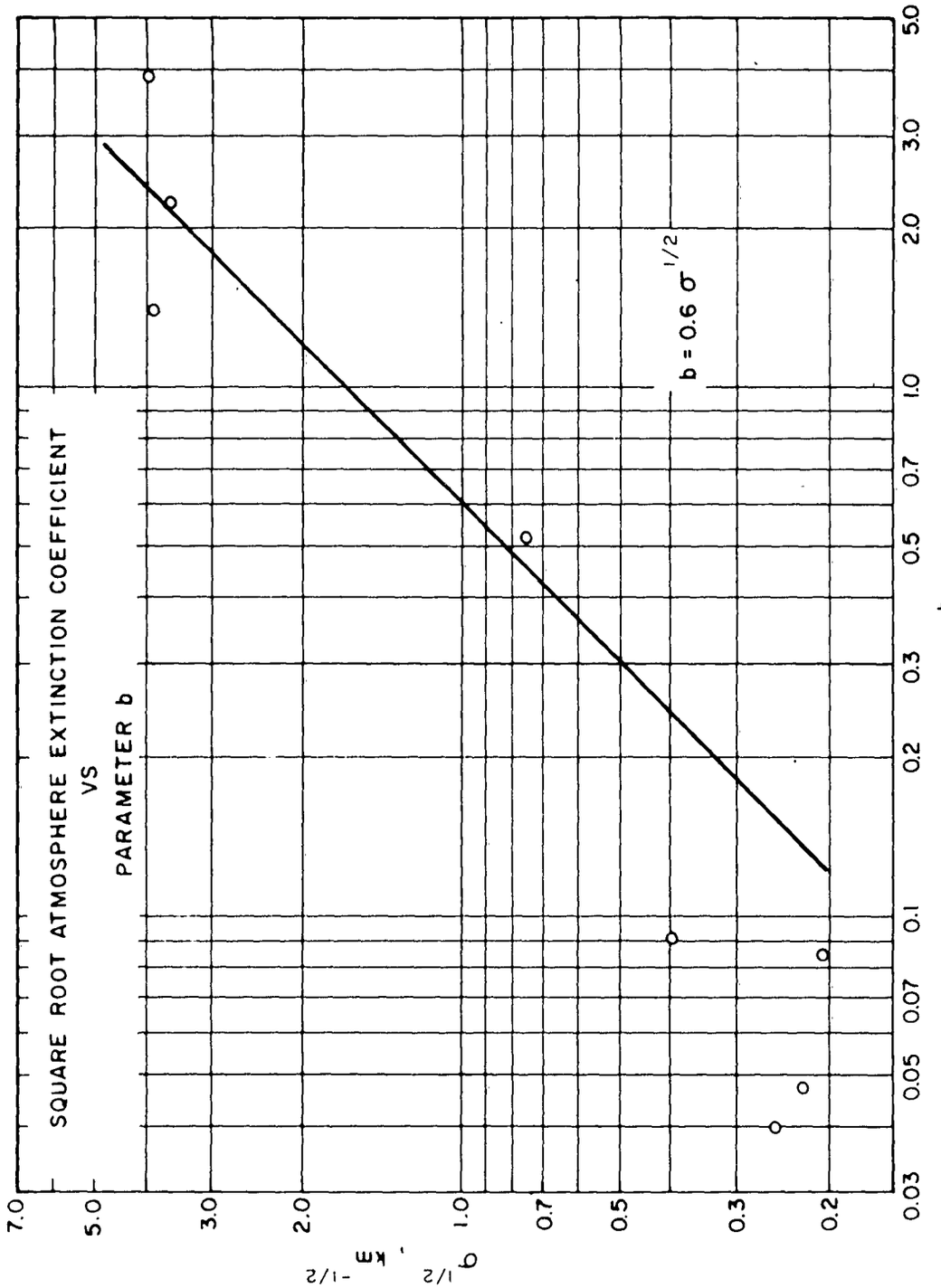
SQUARE ROOT ATMOSPHERE EXTINCTION COEFFICIENT
VS
PARAMETER b
b = 0.6 σ^1/2
q^1/2 , k_E^-1/2
b
7.0
5.0
3.0
2.0
1.0
0.7
0.5
0.3
0.2
0.1
0.07
0.05
0.03

FIGURE 16

$$b = 0.6\,\sigma^{1/2} \tag{4.6}$$

Substitution of equations (4.5) and (4.6) into equation (4.4) yields an expression for the total flux from an isotropic source in terms of the atmospheric extinction coefficient and the distance:

$$T = \frac{e^{-\sigma R}}{R^2} + \frac{0.6\,\sigma^{1/2}\, e^{-\sigma^{1/3} R}}{R} \tag{4.7}$$

Equation (4.7) is empirical, and as such has limitations in its use. Considering its derivation - i.e., the approximate relationships between the measured characteristic of the eight atmospheres - it seems reasonable to assume that this equation is useful for atmospheric extinction coefficients from $0.02 < \sigma < 20\ km^{-1}$.

The usefulness of equation (4.7) for computing the scattered flux is illustrated in Figure 17. The quantity SR vs the slant range, R, is plotted for the experimental data (reproduced from Figures 7 to 14) at the left. At the right, the computed values of SR are plotted for comparison. It can readily be seen that the computed scattered flux approximates the general trends quite satisfactorily; the slopes of the curve, with the exception of the three light hazy atmospheres, are well reproduced. The magnitude of the observed scattered flux in haze appears to be low. A reasonable explanation is that this flux is small, and as such approaches the magnitude of the background. The evaluation of the scattered flux as it approaches the magnitude of background requires more than the simple densitometric techniques used in this preliminary study. As the optical density of the scattering atmospheres increases, there is a commensurate increase in the amount of scattered flux, and therefore less apparent deviation between the experimental and calculated scattered fluxes.

It is useful to compare the total transmissions predicted by equation (4.7) with the corresponding observed quantities for the various atmospheres. The total energy transmissions were obtained from the experimental data by adding the direct and scattered fluxes, DR^2 and SR^2, appearing in Figures 7 through 14. Values at each range were averaged and plotted on Figure 18. Curves were also drawn on Figure 18, representing the predictions of equation 7 for each of the transmissions. Agreement between experimental and predicted values is good.

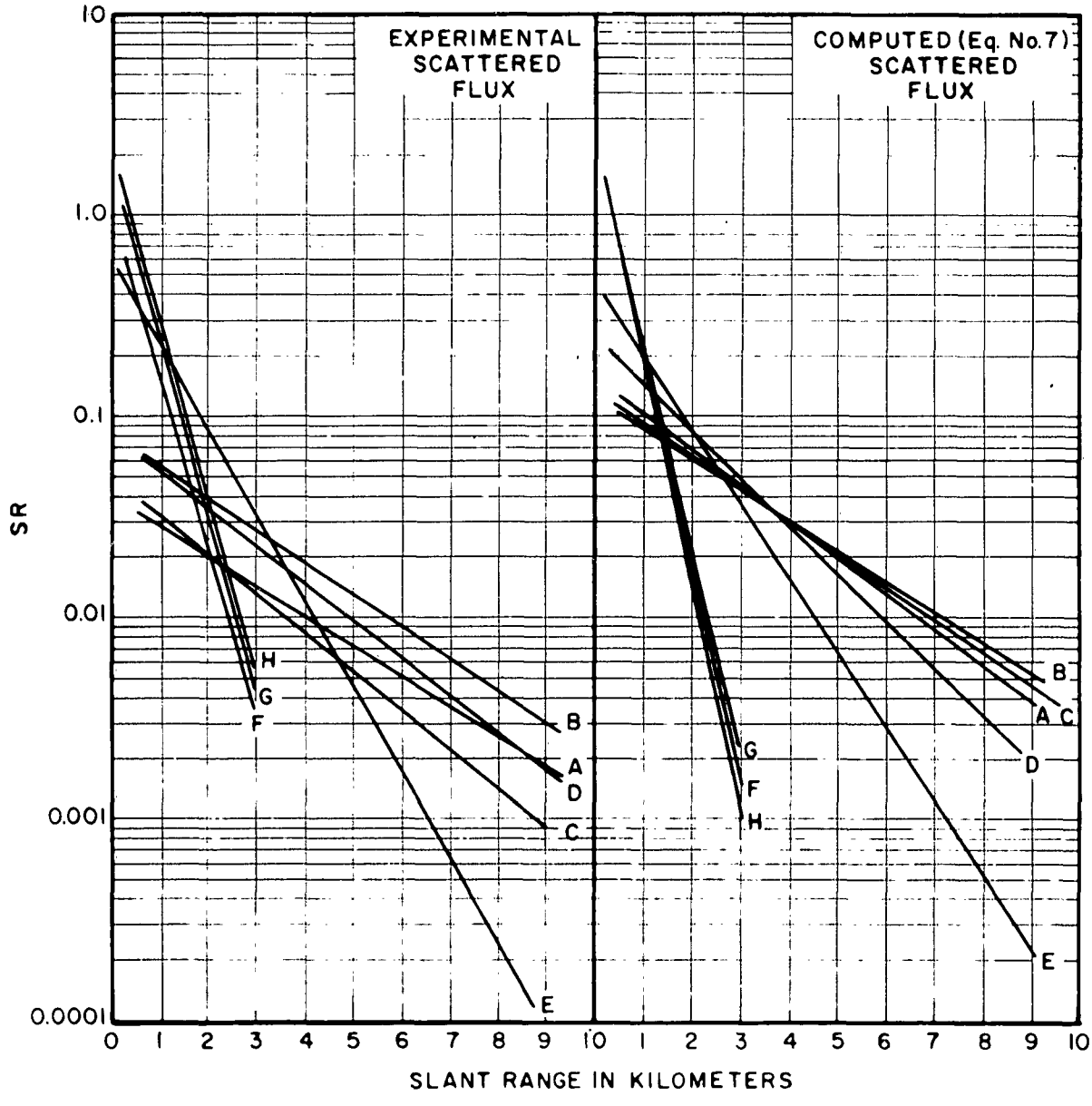
EXPERIMENTAL SCATTERED FLUX
COMPUTED (Eq. No.7) SCATTERED FLUX
SR
10
1.0
0.1
0.01
0.001
0.0001
0 1 2 3 4 5 6 7 8 9 10
1 2 3 4 5 6 7 8 9 10
SLANT RANGE IN KILOMETERS
A
B
C
D
E
F
G
H

FIGURE 17

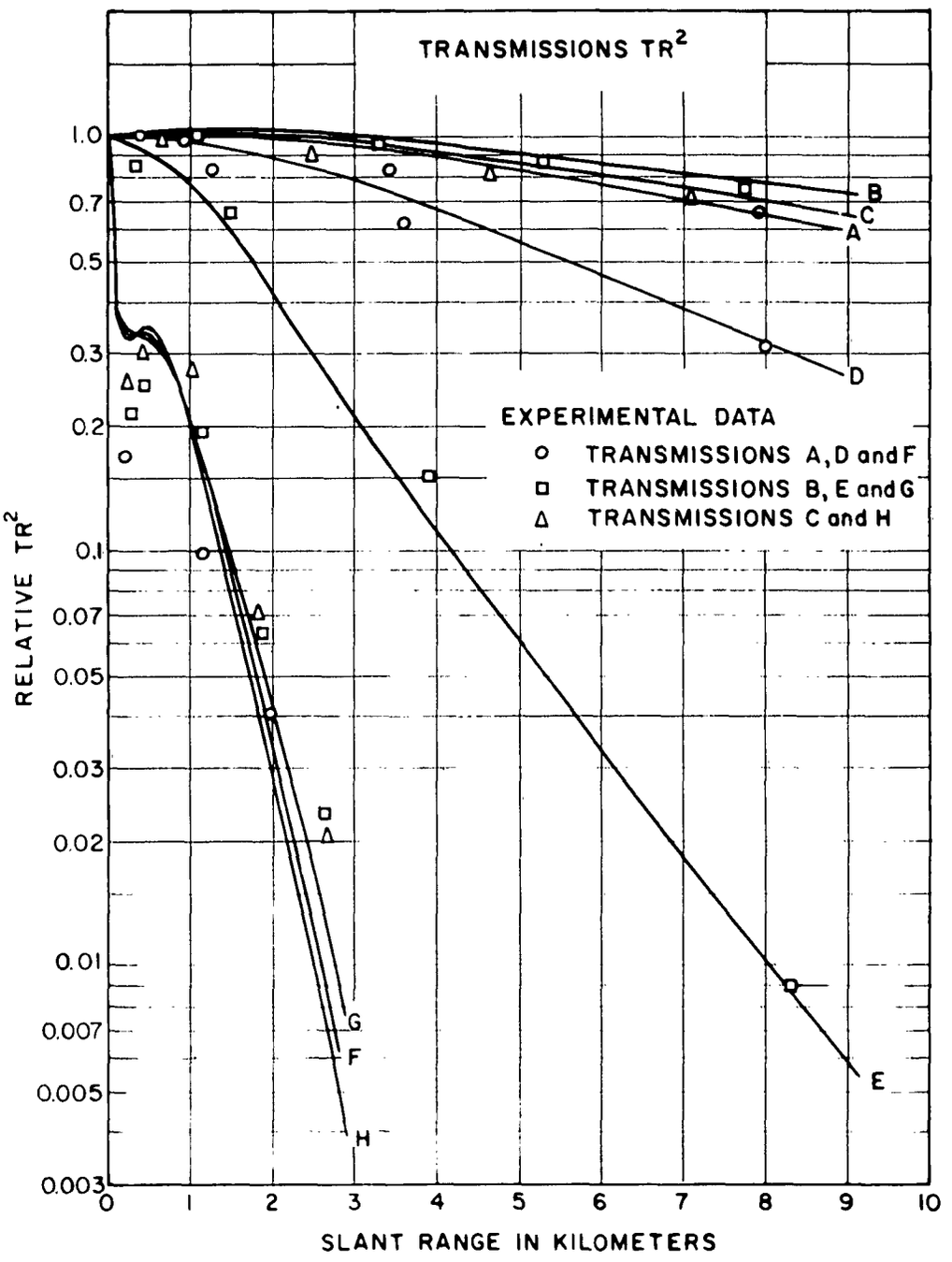
TRANSMISSIONS TR²
EXPERIMENTAL DATA
TRANSMISSIONS A, D and F
TRANSMISSIONS B, E and G
TRANSMISSIONS C and H
RELATIVE TR²
SLANT RANGE IN KILOMETERS
1.0
0.7
0.5
0.3
0.2
0.1
0.07
0.05
0.03
0.02
0.01
0.007
0.005
0.003
0
1
2
3
4
5
6
7
8
9
10
A
B
C
D
E
F
G
H

FIGURE 18

V. ANGULAR DEPENDENCE OF SCATTERED ENERGY

The aureole is a characteristic phenomenon when light sources are viewed through hazy or foggy atmospheres. The aureole is, of course, a manifestation of light scattered by atmospheric aerosols. The photographic technique described earlier in this report yields information on the angular distribution of brightness about the spherically symmetric photoflash sources observed under various conditions of atmospheric optical densities. It is the aim of this section to examine the angular distribution of brightness for variability, for significant parameters, and for consistency (when integrated, this brightness function must yield the total scattered flux.)

Theoretical studies of the angular dependence of scattered flux have been based on the relationship between the scatterer and the wavelength of the incident radiation, i.e., on the Mie theory. Examples of this approach have been reported by Chu and Churchill, Lowan, Van de Hulst (References 7, 8 and 9) and others. Unfortunately, it is quite difficult to apply this theory to the experimental data because droplet sizes are unknown, and because of the wide range of atmospheric optical densities measured. For this reason the approach is empirical.

An examination of the angular data indicates that the brightness of the aureole varies as much as four orders of magnitude above background. A large amount of scatter was observed when all of the data obtained was considered, although each individual photographic film showed a regular decrease of brightness as the angle from the source increased.

It is also evident that if the distance from source to observer is maintained constant, an increase in the optical density of the atmosphere decreases the brightness of the aureole near the source, but increases the angular size of the aureole. This trend is clearly illustrated as one makes the transition from moderate smoke and haze to fog. It is not apparent from these measurements that this trend is continued as the transition is made from moderate smoke and haze to light haze. Alternate explanations for this change in trend can be sought; the first being, of course, that for light haze the aureole near the source is, in fact, less bright than the aureole at the same angle when observed in moderate haze. This point of view is supported if one postulates that the particle size distribution remains constant and that only the concentration of scatterers increases as the turbidity increases from light haze to moderate haze and smoke.

A second explanation for the observed increase in brightness near the source as the optical density of the atmosphere increases (although the mean free path is still long) attributes this increase to the manner in which the brightness measurements were made. The densitometer available to this project had an aperture that was too large to yield approximately incremental fluxes when measuring aureoles of small angular extent. In the analysis of light hazes, where the brightness falls off very rapidly with angular distance, the average flux over a finite incremental angle may be a poor approximation to the brightness at points near the source. This effect, plus the **deliberate** defocussing of the cameras, produced an average flux that is less than the maximum of flux per unit solid angle received over the incremental angle.

The uncertainty attendant on the brightness measurements made in light haze has resulted in our concentrating attention quantitatively on the trends from moderate dense haze and smoke, to fogs. This range of turbidity is the region where the aureole is prominent and changes brightness and size most markedly. It is, therefore, the region of greatest interest both in theory and in application.

In analyzing the data of brightness as a function of observer angle, the following line of reasoning was used. Starting from the subjective impression that the aureole appeared as a luminous mantle surrounding the source, particularly when viewed at an appreciable distance, the brightness data taken from the photographs were plotted as a function of the apparent lateral distance from the source. This distance is given by R sin Θ, where R is the source-to-observer distance, and Θ is the angle, subtended at the observer, between the direction of the source and the direction in which brightness was measured (see Figure 19). Since the aureole is presumably spherically symmetrical, observation at a given value of R sin Θ always represents the same path through it; the only difference between data points is that the path length increases with increasing distance from the source.

The empirical relationship between brightness, B, and the lateral distance from source, R sin Θ, is shown in Figure 20, where log B is plotted against log $(R \sin \Theta)^2$. Each curve represents the brightness distribution under given meteorological conditions and at a given distance from the source. Most of the curves tend toward finite maxima at low values of R sin Θ, and increase in uncertainty at larger values of radial distance from the source, where the brightness merges into the background.

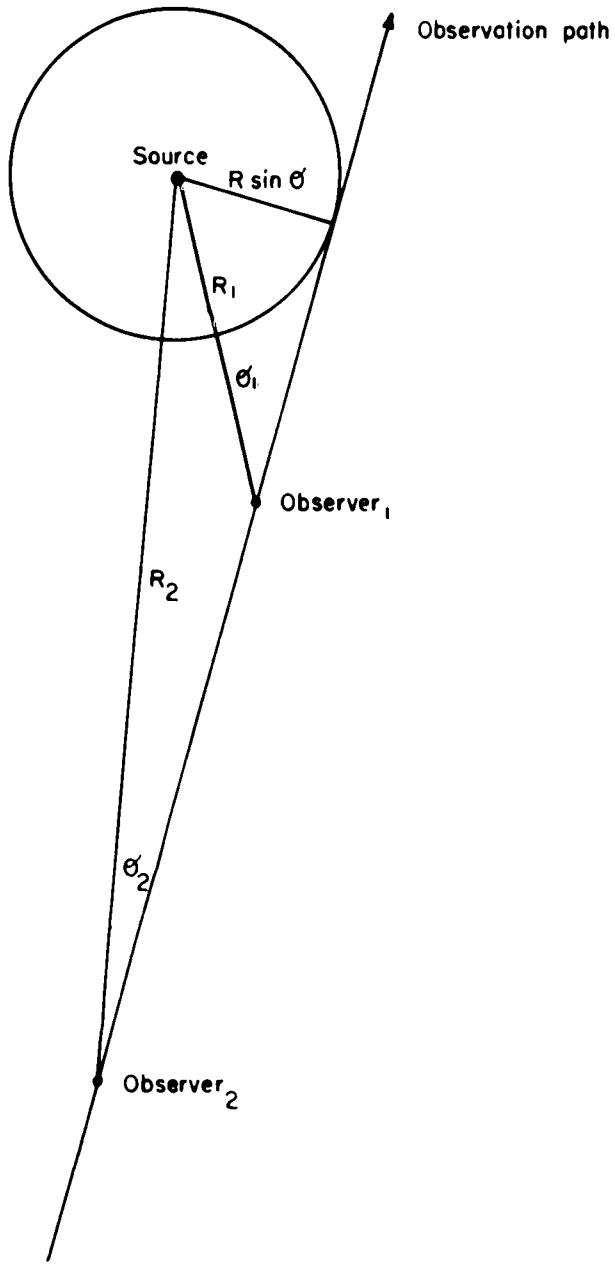

FIGURE 19

BRIGHTNESS VS DISTANCE AND DIRECTION

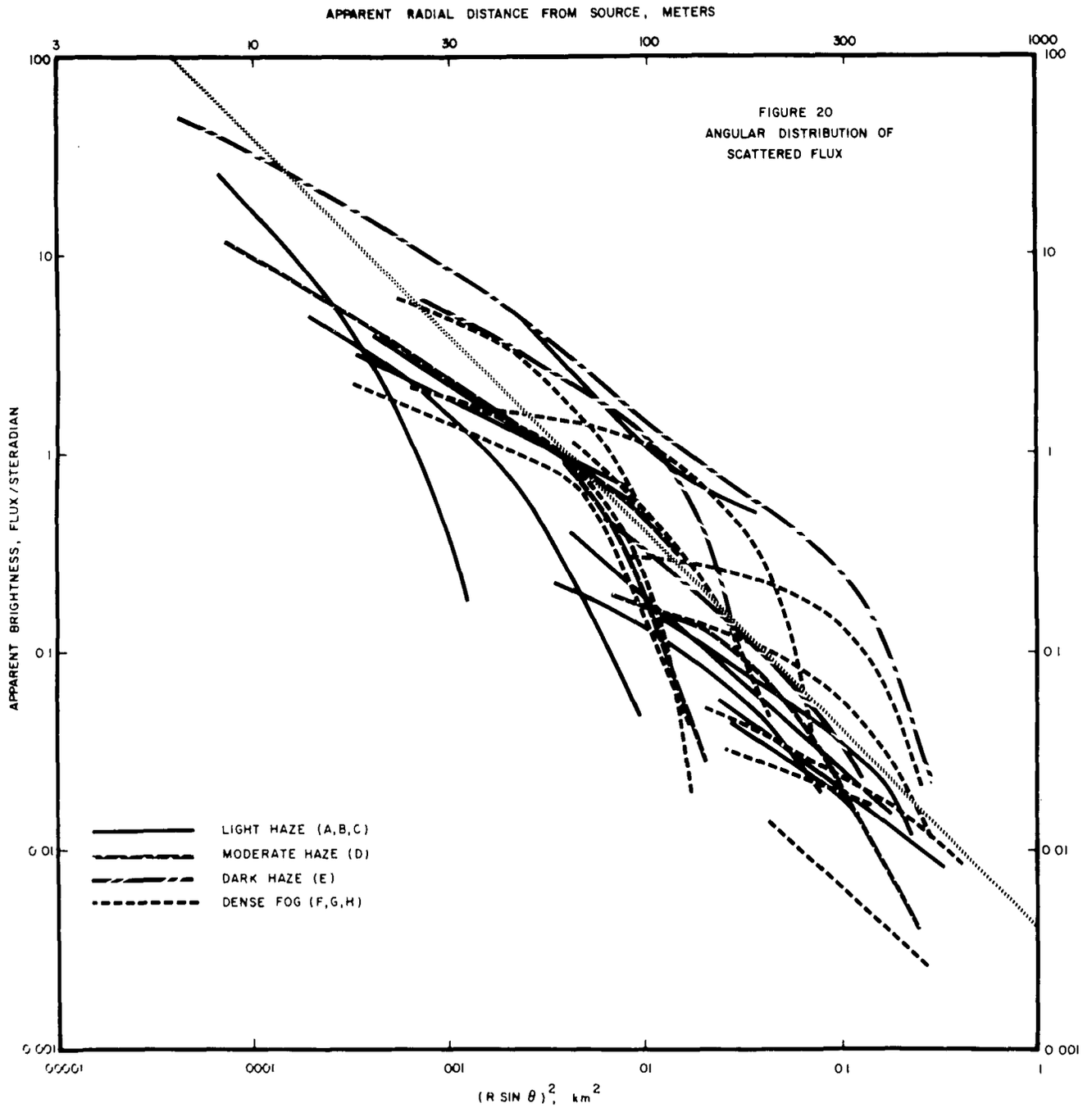

FIGURE 20
ANGULAR DISTRIBUTION OF
SCATTERED FLUX

It can be seen that in spite of the fact that the individual curves are not straight and do not necessarily approximate a 45^{o} slope, the aggregation follows such a relationship. Within a factor of 3, the bulk of the data can be represented by a 45^{o} line independent of atmospheric conditions, or, analytically

$$B = \frac{0.004}{R^2 \sin^2\Theta} \quad \text{flux per steradian} \tag{5.1}$$

where R is expressed in kilometers.

The fact that this relationship covers a range of over four decades of brightness (normalized only to a standard source) and visibilities varying from 0.3 to 100 km is in itself a remarkable finding. With it, one can calculate the amount and angular distribution of scattered energy transmitted through any scattering atmosphere from an arbitray source geometry, and obtain an answer good to a factor of three. (It should be noted that the direct beam contribution must be computed separately to obtain the illumination of the observer).

This expression for the brightness distribution can, of course, be integrated to obtain the total scattered flux at any point. From the definition of brightness, the flux received on a unit area of a flat detector is given by:

$$S = \int B \cos\Theta \, d\Omega = \pi \int_{\sin^2\Theta_o}^{\sin^2\Theta_1} B \, d(\sin^2\Theta) \tag{5.2}$$

when the detector face is oriented normal to the line joining source and detector, and assuming the aureole to be circularly symmetrical about the source. Here Θ_o represents the minimum angle of observation, in this case the angle set by the defocusing of the cameras, and Θ_1 the maximum angle. Because the brightness decreases rapidly with angle, this maximum may be assumed to be $\sin\Theta_1 = 1$. Introducing the emperical brightness relationship and integrating,

$$S = \frac{0.004\,\pi}{R^2} \ln \frac{1}{(\sin^2\Theta_o)} \tag{5.3}$$

From the known camera constants and the amount of defocusing, this works out to be:

$$S = 0.1/R^2 \tag{5.4}$$

This result is at variance with equation (4.3), obtained by graphical integration of the scattered light appearing in each of a series of photographs observing a given flash. However, within the error of a factor of three given above, the equations are in agreement over the applicable range. An idea of the approximations involved may be gained by inspection of Figures 7 through 14; equation (5.4) predicts that $SR^2 = 0.1$, which is very roughly descriptive of the course of the data.

Integration of the angular flux distribution thus reveals that the relationship given by equation (5.1) is only an approximation, though a very useful one for giving the qualitative characteristics of the aureole distributions. It is believed that further observations will be required to produce more refined relationships. However, those reported here should be sufficient to permit rough calculations to be made of the flux which would penetrate openings of particular orientations and solid angles.

VI. CONCLUSIONS

The preliminary atmospheric transmissions determined with the photographic technique were made in atmospheres covering a wide range of visibilities. From these eight transmissions it has been possible to derive an empirical relationship between the scattered and direct flux extinction coefficient. From this, an empirical equation for the total transmission from an isotropic source may be computed, as it was shown in Section IV, equation (4.7):

$$T = \frac{e^{-\sigma R}}{R^2} + \frac{0.6\,\sigma^{1/2}\, e^{-\sigma^{1/3} R}}{R} \qquad (4.7)$$

In equation (4.7) the two independent variables are the range in km and the optical density of the intervening atmosphere. The optical density of the atmosphere is expressed as the extinction coefficient. Visibility in km may be substituted for extinction coefficient, σ, using the standard relationship for the visual range:

$$V_m = \frac{1}{\sigma} \ln \frac{1}{C} = \frac{3.912}{\sigma} \qquad (6.1)$$

The standard value of 0.02 is used for C, the threshold of brightness contrast.

The angular distribution of the scattered flux arriving at the observer was likewise derived from the photographs. It was found that the apparent brightness seen by the observer could be approximately related to the apparent radial distance R_r (in km) from the source: within a factor of three, this brightness could be given by:

$$B = \frac{0.004}{R_r^2} \quad \text{flux per steradian} \qquad (6.2)$$

independently of the atmospheric transmission.

The empirical expressions constructed for the direct, total scattered, and angular distribution of flux lead to precise statements of the conditions under which the scattered flux predominates over the direct flux. For atmospheres where the visibility is less than 4 km (i.e. $\sigma > 1\ \text{km}^{-1}$), the scattered flux becomes equal to the flux in the direct beam

somewhere at a range that is less than 1.5 km. It is only under conditions of good visibility that scattered flux is not a significant fraction of the total radiant energy. As a rule of thumb, the direct beam contributes the main fraction of the radiant energy when visibilities are greater than 40 km ($\sigma = 0.1\ km^{-1}$) while flux contribution from the direct beam may be neglected in respect to the contribution from the scattered flux for visibilities less than 0.4 km ($\sigma = 10\ km^{-1}$). For intermediate visibilities, both the direct and scattered flux must be considered in estimates of the total flux. In this range of visibility, the fraction of each flux that will be received by a given detector depends not only on the extinction properties of the atmosphere (i.e, σ dependent) but also on the distance from the source at which the measurement is made (i.e., R dependent).

As an illustration of the σ and R dependence, consider what type of atmosphere scatters the greatest amount of energy to a fixed detector. This question can be answered by considering equation (4.7). Differentiating the second term with respect to σ, keeping R constant, and setting the resulting expression equal to zero, the functional relationship becomes:

$$\sigma = \left(\frac{3}{2R}\right)^3 \tag{6.3}$$

Equation (6.3) states that the atmosphere scattering the greatest amount of flux to a detector depends not only on the extinction properties of the atmosphere, but also on the distance between detector and source. For example, a detector 1 km from the source would receive the greatest amount of scattered flux from an atmosphere where $\sigma = 3.4\ km^{-1}$. Range, in addition to the extinction coefficient, enters into a proper description of the properties of a scattering atmosphere.

Enough work was done with the photographic technique to establish its utility as a method for studying light scattering in the atmosphere and to show where it needed improvement to yield more precise results. It is believed that further measurements with brighter sources, more accurate distance determinations, and better densitometry equipment will permit firmer conclusions to be drawn about the scattering properties of real atmospheres.

REFERENCES

1. R.G. Eldridge and J.C. Johnson, "Experimental Measurements of Diffuse Transmittance in Real Atmospheres," Report No. TOI 56-30, Final Report on Contract No. AF 19(604)-988, 60 pp., December 1956.

2. R.G. Eldridge and J.C. Johnson, "Diffuse Transmission through Real Atmospheres." JOSA 48, 463-468 (1958).

3. Kodak Data Book, 7th Edition, Kodak Films, 1956.

4. A.R. Greenleaf, Photographic Optics, The MacMillan Corp., New York, N.Y., 1950.

5. E.T. Clarke and P.I. Richards, "Scattering of Gamma Rays Near an Interface," AFSWC-TR-57-3 Appendix.

6. W.E.K. Middleton, "The Effect of an Angular Aperture of a Telephotometer on Telephotometry of Collimated and Non-Collimated Beams," J.O.S.A., 39, 576-591 (1949).

7. C.M. Chu and S.W. Churchill, "Representation of Angular Distribution of Radiation Scattered by Spherical Particles," J.O.S.A. 45, 958-962, (1955).

8. A.N. Lowan, "Table of Scattering Function for Spherical Particles," N.B.S. Appl. Math. Series 4, U.S. Government Printing Office, Washington, D.C. (1948).

9. H.C. van de Hulst, Light Scattering by Small Particles, John Wiley and Sons, New York, New York, 1957, 470 pp